The Effects of Gamma (γ-) Sterilization on the Redox Stability, Minerology, and Physicochemical Properties of the Synthetic Iron Oxides Ferrihydrite, Lepidocrocite, and Goethite.

Brandon Sajad Khan

Thesis submitted to the

Faculty of Graduate and Postdoctoral Studies

in partial fulfillment of the requirements

for the M.Sc. degree in Earth Sciences

Ottawa-Carleton Geoscience Centre

Faculty of Science

University of Ottawa

Abstract

Laboratory analyses were conducted on synthetic iron oxides to assess the use of gamma (γ-) irradiation as an efficient sterilization technique to remove microorganisms present in natural bacteriogenic iron oxides (BIOS) and to determine if the technique induces mineralogical changes within the Fe-rich minerals. Fe-oxides (ferrihydrite, lepidocrocite, and goethite) were synthesized with and without alginate (as a proxy for exopolysaccharides) and microbial reductions were carried out using the bacterium *Shewanella putrefaciens* CN32. A total of 18 Fe-oxide minerals were subjected to microbial reduction to assess redox stability, alteration due to varying levels of gamma irradiation (0, 5, and 28 kGy), and the addition of the exopolysaccharide alginate. Iron reduction rates varied for each Fe-oxide with faster Fe (III) reduction rates observed for the amorphous poorly-sorted 2-line ferrihydrite and slower Fe (III) reduction for the more crystalline Fe-oxides lepidocrocite and goethite. There was no significant impact to the Fe (III) reduction rates due to gamma irradiation ($p > 0.05$), which was confirmed using a t-test for statistical variance between gamma irradiated samples. However, the addition of alginate enabled lepidocrocite and goethite to achieve maximum Fe (III) reduction by an average of 7 days faster when compared to the Fe-oxides synthesized without the exopolysaccharide.

Résumé

Des analyses chimiques ont été faites sur des oxydes de fer synthétiques afin de déterminer si la radiation gamma est une excellente méthode de stérilisation pour éliminer les microorganismes présents dans les oxydes de fer biogéniques naturels et si la technique en soit induit des changements minéralogiques au sein des oxydes de fer. Les oxydes de fer (ferrihydrite, lépidocrocite et goethite) ont été synthétisés (avec et sans alginate utilisé comme proxy d'exopolysaccharides) et ensuite réduits avec la bactérie *Shewanella putrefaciens* CN32. Dix-huit (18) échantillons ont été réduits afin de déterminer la stabilité rédox, les transformations minéralogiques potentielles reliées aux diverses doses de radiation (0, 5, and 28 kGy), ainsi que l'effet de l'alginate sur les taux de réduction. Les taux calculés ont varié pour chaque type d'oxydes. Les taux les plus élevés ont été observés pour la ferrihydrite (un oxyde de fer peu ordonné) alors que les taux les plus bas ont été mesurés pour les oxydes de fer plus cristallins comme la lépidocrocite et la goethite. La radiation gamma n'a pas affecté les taux de réduction de façon significative ($p > 0.05$). Cependant, l'addition d'alginate pendant les synthèses d'oxydes de fer a causé une réduction plus rapide (en moyenne de 7 jours) par rapport aux oxydes ne contenant pas d'alginate.

Acknowledgements

This project could not have been completed without the support of many individuals from different organizations. First and foremost, I'd like to thank my supervisor Dr. Danielle Fortin for her guidance, patience, and support throughout this project. To my colleague Tarek Najem, I owe you many dinners at Nandos as you were there and offered me unparalleled support and dealt with my puzzlement of where the project was going at times. I would also like to thank the Canadian Nuclear Laboratories (CNL) in Chalk River for their help with the sample sterilization.

Special thanks have to go out to my family and friends who supported me along the way. Mom and Grandmami you did a great job of making sure I was fed with copious amounts of food and left overs whenever I was able to make it home for a visit. To the Pollak family, thank you for being a home away from home for the past 10 years. I also owe Agriculture and Agri-Food Canada, specifically Kelly Dean and Andreanne Leger, a huge thank you for making sure I was continuously employed and for being a sounding board whenever I needed it. You both were always there to push me along and give me support, thanks a lot to you both.

There has been a lot of change throughout the course of this project, specifically in the past couple years. That being said, I have not had the chance to dedicate anything to anyone, so I am going to take the opportunity to dedicate this M.Sc. to my Uncle Wazir, Grandmami, and Grandpapi. Enough cannot be said about these individuals and the role they have played and the impact they have had throughout my life. Finally, special thanks to my partner in crime Khalhela Zoeller. You are a gift that I will always cherish.

Table of Contents

List of Figures

List of Tables

1. Introduction

1.1. Minerology of Bacteriogenic Iron Oxides- Ferrihydrite, Lepidocrocite, and Goethite

The finely grained and poorly sorted characteristics of iron (Fe-) oxides enable them to create key mineral assemblages within various geological environments at the Earth's surface and in a range of aquatic environments (Kasama, 2001; Gault, 2011). In the presence of dissimilatory iron-reducing bacteria (DIRB), these oxides can undergo microbial reduction, which has been linked to remedial properties in groundwater and soils (Komlos *et al*, 2007). Over the past two decades, there has been significant research into the role played by bacteria in iron cycling. However, more research and analytical advancement are needed to fully determine the role of microorganisms in their formation and stability, specifically research pertaining to the analytical procedures used to characterize natural bacteriogenic iron oxides (BIOS).

Initial studies have indicated that as most surface waters have a circumneutral pH, ferrous iron (Fe(II)) is chemically unstable thus, causing it to be readily oxidized into insoluble ferric oxides (Fe(III)), which can occur in many different environments within the Earth (Fortin and Langley, 2005). For example, environments in which iron oxides form include: freshwater to marine systems, soils, and to the area of most interest for the purpose of this study, mining impacted environments (Fortin and Langley, 2005; Langley *et al*, 2009[C]). Natural iron oxides are often intermixed with bacterial structures (similar to lithoautotrophic microorganisms), which play a pivotal role in the formation of BIOS, providing a reduction pathway for O_2 and the oxidation of Fe(II) to Fe(III) (Kennedy *et al*, 2011). Iron oxide phases (with respect to colloids) are ubiquitous in the natural environment because iron can occur in a wide variety of minerals and is a common element in most ores (Zänker *et al*, 2003).

Bacteriogenic iron oxides (BIOS) contain Fe (III) - bearing oxides, hydroxides, and/or oxyhydroxides (naturally occurring or that can be synthetically formed) that are formed and precipitated

directly onto or in the proximity of bacterial cells and extracellular substances (e.g. exopolysaccharides), which form aggregates within the environment (Ferris, 2005; Glasauer *et al*, 2001). The minerology of the iron oxides consists of amorphous to poorly ordered 2-line ferrihydrite to the more crystalline phases of lepidocrocite, goethite, and hematite (Châtellier *et al*, 2004; Ferris, 2005). Iron oxides have the tendency to occur as micro and nano-sized particles, which have heterogeneous surface reactivity and high surface to area volume ratio (Cornell and Schwertmann, 2003; Frankel *et al*, 2016).

Such characteristics are what enable iron oxides to be such efficient sorbents of a wide range of trace metals and heavy metals serving as templates for nucleation for the development and growth of metal precipitates (Glasauer *et al*, 2001; Cornell and Schwertmann, 2003; Frankel *et al*, 2016). During precipitation, it is expected that the more amorphous and poorly sorted Fe-oxides will precipitate out first as they are more soluble (e.g. ferrihydrite). However, Fe-oxides, specifically ferrihydrite are likely to undergo phase transformation, which can transform 2-line ferrihydrite to the more crystalline Fe-oxides of goethite, lepidocrocite, hematite, and magnetite due to environmental conditions (e.g. temperature) and the concentration of dissolved Fe (II) (Cornell and Schwertmann, 2003, Glasauer *et al*, 2003).

Past and recent research has also shown that in acidic environments, iron oxidation can also occur due to bacterial metabolism by acidophiles, which derive their metabolic energy from the oxidation of Fe (II) and, as a result, cause the precipitation of ferric minerals (Langley *et al*, 2009[A]). For example, acidophilic iron oxidizers such as *Acidithiobacillus ferrooxidans* have the ability to link iron oxidation to the reduction of electron acceptors in acidic environments, such as mining sites and mine tailings (Langley *et al*, 2009[A]).

Several studies have been carried out looking at the chemical and mineralogical transformation of natural BIOS and the fate of their sorbed contaminants under environmentally relative conditions in

the effort to fully understand the role of microorganisms in element cycling and mineral formation (Fortin and Langley, 2005).

Recent research has suggested that a crucial step pertaining to the sterilization process of BIOS samples collected may be causing alteration to the reduction potential of natural ferric oxide versus synthetic hydrous ferric oxide (HFO), thus potentially affecting the crystallinity, mineralogy, surface chemistry/composition, and its overall structure (Cismasu *et al*, 2013). Therefore, the main goal of the present study is to continue to further investigate element cycling and mineral formation (specifically synthetic bacteriogenic iron oxides) and delve into the impacts of the gamma (γ-) sterilization (an analytical procedure) and its effect on the reduction potential and geochemical processing of synthetic 2-line ferrihydrite ($Fe_5HO_8 \bullet 4H_2O$), lepidocrocite (γ-FeOOH), and goethite (α-FeOOH).

1.2. Sterilization methods

There has been much research done since the early 1980's that have assessed many different sterilizing methods that can be used for soil and sediment samples to remove or reduce biological activity (McNamara *et al*, 2003). Samples are subjected to sterilization to ensure that the observed reduction rates are not affected by microbial communities, which is also important in the field of remediation (Langley *et al*, 2009[A]). Many studies have suggested that of all the sterilization methods (hot air, chloroform, methyl bromide, propylene oxide, autoclave, and formaldehyde), gamma (γ-) irradiation has been proven to be the most effective (McNamara *et al*, 2003). Gamma-irradiation results in minimal secondary effects on soil and sediment samples whilst causing little physical and mineralogical alterations to the samples of interest and is deemed the safest approach for sterilization in the medical and food industries (McNamara *et al*, 2003; Ramsay and Bawden, 1983; Brown *et al*, 2014).

However, as research has progressed on gamma-sterilization, some studies have shown that gamma-sterilization effects metal and metalloid remobilization along with changes of the

physicochemical properties of the minerals (McNamara *et al*, 2003; Bank *et al*, 2008). Schaller *et al* (2011) determined that there was higher remobilization of uranium (U) and arsenic (As) in samples subjected to sterile treatment after ten days which was accompanied by a higher concentration of dissolved organic compounds (DOC), manganese (Mn), and iron (Fe) when compared to untreated samples. It was also noted by Schaller *et al* (2011) that there was a change to the physicochemical properties of the sediment samples when gamma-radiation was used for sterilization if the samples contained a high organic content.

In most sample types (e.g. soil, sediment, liquid etc.), a low dose of gamma-irradiation (<50 kGy) is needed for the removal of microorganisms (Bank *et al*, 2008). Buchan *et al* (2012) list gamma-irradiance with the following expected outcomes: 5 kGy (no nematodes), 10 kGy (no fungi), 20 kGy (only bacteria), and 40 kGy (no microbial biomass at all). However, at high doses of gamma-irradiation (>70 kGy), changes have been observed with respect to the sediment mineral chemistry and dissolved organic matter content (Bank *et al*, 2008; Buchan *et al*, 2012). Changes that can occur include: reduction of Fe (III) to Fe (II) (induces redox processes on lattice iron), alteration to the solubility of clay minerals, and the reduction of the dissolved organic concentrations (Bank *et al*, 2008; Plotze *et al*, 2003).

While gamma-irradiation is used on a global scale as a sterilization process for sediment and soil samples, its influence on the geochemical and physicochemical properties of iron oxides is a crucial area to help better understand for the fields of remediation, environmental science, and geomicrobiology. In addition, radiation dose requirements essentially affect the reduction potential of the iron oxide samples (Bank *et al*, 2008). The determination of an optimal threshold will be needed to pinpoint the amount of radiation to completely differentiate at which point microorganisms are being removed from the iron oxide samples and at which point there is alteration to the physicochemical properties of the minerals (McNamara *et al*, 2003; Gournis *et al*, 2000).

1.3. Hydrolysis and Radiolysis

Gamma radiation is an ionizing radiation and when used as a sterilization technique can cause the dissociation of water molecules creating several chemical species (e.g. e_{aq}^-, HO•, H•, HO_2•, H_3O^+, OH^-, H_2O_2 and H_2) (Dzaugis et al, 2015). Therefore, there is an increased chance of producing more radicals with the addition of the exopolysaccharide alginate due to the large carbon chain, increased hydrogen atoms and hydroxyl groups, all of which can have a negative impact on the reduction rates of the synthetic BIOS secondary mineralization along with the minerology of the synthetic Fe-oxides (McNamara *et al*, 2003; Caër, 2011). Radiolysis occurs within any system that when sterilized there is water present and is in contact with gamma radiation. Radiolysis is quite ubiquitous within the fields of geology, chemistry and biology and is also present within the food and medical industries because gamma radiation is used as a sterilization technique for agri-foods products along with medical and pharmaceutical equipment (Lamm, 2007; Piri *et al*, 2011).

1.4. Objectives

This thesis fits into a larger project designed to assess the role played by dissimilatory iron reducing bacteria (DIRB) in iron cycling within sediments that have overtime been impacted by mining activities and the competition between sulfate-reducing bacteria (SRB) and DIRB. The objectives of the present project are to (1) enhance the analytical procedure of sample preparation by investigating γ-sterilization and its effect on the physio-chemical properties of synthetic BIOS samples ferrihydrite (Fh), lepidocrocite (Lep), and goethite (G) within a laboratory setting; (2) determine the impact that γ-sterilization has on the biological properties of the synthetic BIOS samples and compare the Fe (III) reduction rates of synthetic Fh, Lep, and G; and (3) determine the impact of γ-sterilization on the minerology of the synthetic BIOS Fh, Lep, and G and the variation of Fe (III) reduction rates when the exopolysaccharide (EPS) alginate is added during the synthesis protocol.

1.5. Impacts

Better understanding gamma (γ-) irradiation as a sterilization technique and an analytical procedure will aid in the development of an "optimal" gamma-irradiation threshold in which BIOS, water and soil samples can withstand before undergoing physicochemical and mineralogical changes. Synthesis procedures and reduction protocols will contribute to a better understanding of the interactions between Fe-oxides and bacteria and how Fe (III) reduction rates along with redox stability are affected due to gamma irradiation, environmental conditions, and the use of an exopolysaccharide. Due to the sorption properties of Fe-oxides and their interaction with DIRB, this research will add to the body of literature on bioremediation because microorganisms could be used to aid in the rehabilitation during the life cycle of a mining project by promoting mineral formation and sorption. If applied at an industrial scale, this could be used to precipitate metals from the mineral extraction process, tailings ponds, acid mine drainage, and other mineral leachates, which could lead to an improvement in metal recovery and environmental rehabilitation.

2. Materials and methods

2.1. Fe-Oxide Synthesis, Characterization, and Gamma-Ray Sterilization

Abiotic goethite (α-FeOOH), lepidocrocite (γ-FeOOH) and 2-line ferrihydrite (approx. $Fe(OH)_3$) were synthesized using the methods described in Cornell and Schwertmann (2000) (Table 1). All iron oxide minerals were synthesized using a ferric chloride salt ($FeCl_3.6H_20$) (in replicates). Samples were synthesized using $FeCl_3.6H_20$ but in addition, a batch of ferrihydrite with and without alginate was also made with a ferric nitrate salt ($Fe(NO_3)_3.9H_20$) in order to determine whether nitrate would affect the reduction microcosm experiments since the bacterial strains used in this thesis is also capable of reducing nitrate, along with iron. Synthetic BIOS in the presence of alginate were prepared according to the same protocols but in the presence of soluble alginate ($C_6H_9NaO_7$). The mineralogical characterization of all iron oxides samples was confirmed by X-ray diffraction analysis (XRD). Prior to analysis, all iron oxide minerals were dried at room temperature and then ground into a fine powder using a mortar and pestle. The XRD analysis was performed on a *Philips PW 3020 X'Pert Diffractometer* and *Rigaku Ultima IV Diffractometer*, operating at 45 kV and 40 mA using Cu-Kα radiation. The diffraction data were collected over the 10- 70^o 2θ range using a step size of 0.02^o.

Gamma-radiation of the synthetic abiotic and biogenic iron oxides was performed at the Canadian Nuclear Laboratories (CNL) in Chalk River, Ontario, Canada. One set of samples was subjected to an irradiation dose of 5kGy whereas a second set was exposed to 28kGy using a three Category I Cobalt-60 irradiator at the Reactor Chemistry and Corrosion Branch (RCCB) of CNL. The irradiator contained a radioactive cobalt source generating a relatively uniform radiation field with a dose rate of approximately 0.8-1.0 kGy/h.

Scanning electron microscopy (SEM) was done using a JEOL 6610LV-SEM in the Department of Earth and Environmental Sciences at the University of Ottawa. BET Surface area analysis of the various dried iron oxide samples was conducted in the Department of Chemistry at the University of Ottawa,

using a Micromeritics' 3Flex Surface Characterization Analyzer. Prior to N_2 adsorption measurements, powered samples were degassed at a temperature of 50^{o}C under constant N_2 flow for 24 hours.

Table 1: List of Synthetic Fe-oxides that were used for the reduction experiments and the associated range of Gamma Irradiation (0, 5, and 28kGy) along with their abbreviated forms.

Fe-Oxide (Gamma Irradiated-Kilograys (kGy)	Short Form
Ferrihydrite (Non-Gamma)	Fh
Ferrihydrite (5 kGy)	Fh-5kGy
Ferrihydrite (28 kGy)	Fh-28kGy
Ferrihydrite + Alginate (Non-Gamma)	FhA
Ferrihydrite + Alginate (5 kGy)	FhA-5kGy
Ferrihydrite + Alginate (28 kGy)	FhA-28kGy
Lepidocrocite (Non-Gamma)	Lep
Lepidocrocite (5 kGy)	Lep-5kGy
Lepidocrocite (28 kGy)	Lep-28kGy
Lepidocrocite + Alginate (Non-Gamma)	LepA
Lepidocrocite + Alginate (5 kGy)	LepA-5kGy
Lepidocrocite + Alginate (28 kGy)	LepA-28kGy
Goethite (Non-Gamma)	G
Goethite (5 kGy)	G-5kGy
Goethite (28 kGy)	G-28kGy
Goethite + Alginate (Non-Gamma)	GA
Goethite + Alginate (5 kGy)	GA-5kGy
Goethite + Alginate (28 kGy)	GA-28kGy

Mossbauer analysis was also carried out to first confirm the XRD results but also to assess any mineralogical damages caused by gamma irradiation, including the potential reduction of structural Fe (III) by radicals in the biogenic ferrihydrite exposed to 28kGy minerals. The 57Fe Mossbauer spectra were first measured at room temperature using a Topologic Systems MD-222B Mossbauer Spectrometer within a Cu holder with a 1.0cm window to observe the spectra. Samples were analyzed over a 10 hour period to assess isomer shift (IS) and quadrupole splitting (QS). A secondary analysis was carried out for ferrihydrite + alginate gamma irradiated at 28kGy (FhA-28kGy) at 78K to confirm the absence of Fe (II) in the structure of ferrihydrite to ensure no Fe (III) reduction. Samples were kindly analyzed by Dr. Yoichi Sakai Daido and Dr. Yoshio Takahashi at the University of Tokyo, Japan.

Losses on ignition (LOI) experiments were carried out to determine the percent structural water and percent organic matter within the synthetic Fe-oxides. Porcelain crucibles were heated at 375^{o}C in a Lindonberg furnace for 1 hour followed by a cool down period to 150^{o}C. Crucibles were placed in a desiccator for 30 minutes and then weighed. One gram of Fe-oxide "slurry" sample was added to crucibles (pre-ignition weight) and then placed into a pre-heated furnace at 375^{o}C for 24 hours. Once samples were dried and fully heated, they were left to cool to 150^{o}C and then transferred to the desiccator and left to cool to be able to handle (30 min). The Fe-oxide samples were then weighed to determine their post-ignition weight.

$$\textit{Percent Organic Matter (\%OM)} = \frac{\textit{pre-ignition weight (g)} - \textit{post- ignition weight (g)}}{\textit{pre-ignition weight (g)}} \bullet 100 \qquad \textbf{Equation [1]}$$

The determined pre- and post-ignition Fe-oxides values (g) were applied to equation 1 to determine the percent organic matter (%OM) (Table 3). These values along with percent water were used to determine the mg/gdwt of available iron (Table 4).

Percent carbon was also determined at the G.G. Hatch and Stable Isotope Laboratory at the University of Ottawa using the Elemental Isotope Cube (Table 3). Ferrihydrite, lepidocrocite, goethite were dried and crushed into a fine power and placed into tin capsules. Tungstic oxide (WO_3) was added to the capsules (which act as a combustion catalyst and binder, in the case of resilient solids, such as salts, (inorganic) sulphur-bearing minerals, or iron oxides) before being closed. The closed capsules were re-weighed on the microbalance. Calibrated standards were prepared in a range of weights and run with the samples. When loaded, the samples fall into the top of a column of solid chemicals at 1150°C or 925°C where they are flash combusted at 1800°C with the addition of oxygen. Ultra-pure helium is used to carry the resulting gases through the column of chemicals to obtain N_2 , CO_2 , H_2O, and SO_2, then through a series of adsorption traps to separate the gases: "trap and purge" method. A thermoconductivity detector (TCD) measures the gases as they are released.

2.2. Solid Phase Extractions

Abiotic and biogenic ferrihydrite, lepidocrocite and goethite samples were subjected to various chemical extractions to determine the amount of amorphous and crystalline iron oxides (defined as the difference between total iron and amorphous iron). The chemical extraction methodology of Kostka and Luther (1994) was used. Briefly, the treatments included a 0.5 M HCl extraction (extracts ferrous iron and dissolves amorphous iron oxides), an oxalate extraction (extracts ferrous iron and dissolves amorphous iron oxides), an ascorbic extraction (dissolves and reduces amorphous iron oxides), and a dithionite extraction (dissolves and reduces both amorphous and crystalline iron oxides).

2.3. Bacterial reduction experiments of Ferrihydrite, Lepidocrocite, and Goethite

The dissimilatory iron-reducing (DIRB) bacterium *Shewanella putrefaciens* CN32 was used for the reduction experiments. All microcosm experiments were carried out under anaerobic conditions using a Coy Labs anaerobic chamber with an atmosphere of 95:5, N_2:H_2. The chemically defined growth medium (CDM) and reduction protocol of Langley *et al*, (2009) were followed (Appendix E).The microcosms contained 4 mM of Fe (in the form of abiotic iron oxide or alginate iron oxide) and 3.9 mM of PO_4. The bottles (in triplicate) were sampled at time zero (t0), after 3 hours (t1) and 6 hours (t2) on the first day and then every 24 hours for the remainder of the experiment, which ranged from 14 -40 days depending on the Fe-oxide. Sub-samples were collected for the analysis of total soluble Fe (II) and total soluble Fe (III) (using the ferrozine method of Stookey, 1970) and pH and Eh measurements and bacterial counts were determined as outlined in Langley *et al*, (2009). Control (abiotic) microcosms containing no bacteria were also set up and sampled for the same parameters as the ones containing *S. putrefaciens* CN32. Reduction rates were calculated using the linear equations produced from the percent proportions of Fe (III) to Fe (II) post-inoculation using the ferrozine curve (Stookey, 1970; Langley *et al*, 2009; Glasauer *et al*, 2003). Reduction rates follow the enzymatic first order kinetic model of Michaelis-Mention that studies the enzyme (*S. putrefaciens* CN32)-substrate (Fe-oxide) complex to

generate the product and to regenerate the free enzyme (Berg *et al*, 2002). The minimum and maximum Fe (III) to Fe (II) proportions were used to create the linear plot to determine the Fe (III) reduction rate.

Prior to use, bacterial cells were stored in a tryptic soy broth (TSB) at 4^{o}C and then once ready to use, they were plated and maintained on tryptic soy agar (TSA) at ambient temperature. Reduction experiments were carried out in microcosms consisting of a chemically defined medium (CDM), which was composed of 20mM sodium lactate, 3.5 mM sodium phosphate, 4mM 1.4-piperazinediethanesulfonic acid (PIPES) buffer, and a trace metal salt solution. After 48 hours of growth, single colonies from the TSA plate were subjected to a series on CDM: TSB mixtures (50:50, 95:5, and 99:1) to allow CN32 to acclimatize to the conditions of the chemically defined medium. For each subculture phase, the CDM: TSB mixtures were incubated for 24-36 hours at ambient temperature on a rotary shaker at 125-130 rpm. Following the 99:1 mixture of CDM: a TSB subculture (4 mL of mixture) was added to a 100 mL sterile flask (autoclaved with magnetic stir-bar) and incubated on a stir-plate at moderate-high rotation speed at ambient temperature for 48 hours. The concentrated cell suspensions were then harvested by centrifugation (50 mL centrifuge tubes) and re-suspended using a small volume (2 mL) of sterile 100% CDM. This final cell suspension was used for the reduction experiments within the microcosms.

The inoculation volume of the concentrated cell suspension for the reduction experiments was determined by using a protein assay dye agent (BioRad Protein Assay II) and serial dilutions. Using the Ultraspec 1100 spectrophotometer (wavelength set at 595 nm), the absorbance was applied to equation [2] to determine the final amount of cell suspension needed for the reduction experiments. The equation for the determination of *Shewanella putrefaciens* CN32 needed for inoculation is outlined in equation 2.

$$\textbf{Amount of CN32 (µL)} = \frac{\textbf{(0.05) (700mL)}}{\textbf{(Average Measured Absorbance)}} \qquad \textbf{Equation [2]}$$

2.3.1 Bacterial reduction experiments of Ferrihydrite to Test for the effects of Sunlight and Age of the *Shewanella putrefaciens* (CN32) inoculum during the Microbial Reduction Experiments.

Batch samples of Fh and FhA were synthesized using the ferric chloride salt solution mentioned above. To determine whether there was an effect from sunlight onto the reduction experiments within the biotic microcosms, sample bottles (control and triplicates) were wrapped in aluminum foil to ensure there was no interaction with UV-radiation. Microcosm experiments were sampled using the same procedure mentioned in Section 2.3.

The Fe-oxide slurry of the Fh and FhA batch used for the reduction experiments to test the exposure to sunlight was also used in the microcosms experiments in order to determine whether there was an effect on the reduction rates of Fh and FhA when there was addition of freshly inoculated *Shewanella putrefaciens (CN32)*. *Shewanella putrefaciens* was inoculated and inputted into each microcosm in triplicates following the same procedure outlined above. The difference was in the time in which the *Shewanella putrefaciens* was transferred from inoculation to the microcosm. To test the effect of new *Shewanella putrefaciens* cells on the reduction of the Fe-oxide in the microcosm (following the 100% inoculation period in CDM), the inoculum was transferred directly to each microcosm after a series of washings before the reduction experiment commenced. To test the ageing of *Shewanella putrefaciens*, the concentrated CN32 was stored in the fridge for 5 days prior to being added to each microcosm and the reduction experiments commenced.

3. Results

The following chapter focuses on analyses and results collected through this thesis. The reduction potential (Eh) (corrected with respect to the reference hydrogen electrode), pH, total ferrous and ferric iron were measured during the microbial reduction of 18 Fe-oxide minerals over a period of 17 to 28 days (mineral dependent). Characterization and raw data during this process can be found in the respective appendices.

3.1. Iron Oxide Characteristics and BET Analysis

The mineralogy of ferrihydrite ($Fe(OH)_3$), lepidocrocite (γ-FeOOH), and goethite (α-FeOOH) was confirmed using X-Ray Diffraction (XRD) (Appendix A-1 to A-3) and compared to the spectra in Cornell and Schwertmann (2003). The diffraction patterns for the poorly ordered 2-line ferrihydrite (Appendix A-1) displayed two distinctive broad reflections at d-spacings of ~2.5 and 1.5 Å, which are characteristic of 2-line ferrihydrite and there are no other visible patterns to suggest that any transformation (to the more crystalline structures of goethite and lepidocrocite) occurred during the synthesis procedure, in the presence of gamma irradiation (5 and 28 kGy), and when alginate was added to the system. The same can be concluded for goethite and lepidocrocite (samples with the addition of alginate and gamma sterilized) that the mineralogical structures of both minerals were not altered (Cornell and Schwertmann, 2003). The 11 distinctive peaks for goethite and the 18 for lepidocrocite were clearly displayed.

Mossbauer analysis (Appendix F) further confirmed the mineralogical structure for Fh, Fh-28kGy, FhA, and FhA-28kGy. The analysis at room temperature (293K) reported the following values for ferrihydrite: isomer shift (IS) = 0.351 mm/s, quadruple splitting (QS) = 0.703 mm/s and IS= 0.344 mm/s, QS= 0.748 mm/s, which are similar to the outlined values in Cornell and Schwertmann (2003) ((IS) = 0.35 mm/s, QS = 0.72 mm/s and IS= 0.34 mm/s, QS= 0.79 mm/s). The values for IS= 0.35 mm/s shows high spin Fe^{3+}in octahedral symmetry in oxygen-coordinated species and IS= 0.34 mm/s corresponds to high

spin Fe^{3+} in tetrahedral oxygen-coordinated species. Mossbauer analysis was also carried out at low temperature (78K) and the spectrum revealed only the presence of Fe (III) and no Fe (II) (which can be missed at the room temperature analysis), further confirming the mineralogical structures of FhA, and FhA-28kGy. The analysis at low temperature reported the following values for ferrihydrite: IS = 0.35 mm/s, QS = 0.738 mm/s and IS= 0.462 mm/s, QS= 0.766 mm/s, which are also similar to that of Cornell and Schwertmann (2003).

Scanning electron microprobe analysis (Appendix B) revealed that after the addition of the exopolysaccharide alginate, the iron particles formed larger aggregates than the non-alginate ones. The original spherical shape of ferrihydrite became more hexagonal and packed (Appendix B-1) with more aggregates, while lepidocrocite changed from a lath-shaped elongated crystal to a more cubic and blocky face (Appendix B-2), and goethite underwent a particle change from small crystalline masses to more blocky masses stacked in layered sheets (Appendix B-3).

BET analysis determined a surface area of 95 and 293 m^2/g for ferrihydrite and ferrihydrite + alginate, 70 and 121 m^2/g for lepidocrocite and lepidocrocite + alginate, and 64 and 200 m^2/g for goethite and goethite + alginate, respectively. The results indicate that the addition of the exopolysaccharide alginate increased the surface area of the alginate-iron-oxides, however all values fall within the literature range (Cornell and Schwertmann, 2003) (Table 2).

Table 2: BET Analysis results for Ferrihydrite ($Fe(OH)_3$), Lepidocrocite (γ-FeOOH), and Goethite (α-FeOOH) (with and without Alginate) compared to literature values.

BET Analysis-Surface Area (m^2/g)		
Mineral	**Sample Surface Area Values (m^2/g)**	**Literature Range- High Surface Area (Cornell and Schwertmann, 2003) (m^2/g)**
Ferrihydrite (Fh)	95	100-700
Ferrihydrite + Alginate (FhA)	293	100-700
Lepidocrocite (Lep)	70	15-260
Lepidocrocite + Alginate (LepA)	121	15-260
Goethite (G)	64	8-200
Goethite + Alginate (GA)	200	8-200

Table 3: Loss on Ignition (LOI) results for Ferrihydrite (Fe $(OH)_3$), Lepidocrocite (γ-FeOOH), and Goethite (α-FeOOH) (with Alginate) used to determine the Percent Structural Water and Percent Organic Matter along with Percent Carbon determined by Elemental Analysis. Values include standard deviations.

Mineral	% Stoichiometric Water Present	% Actual Water Present (No Alginate)	% of Water in Fe and Alginate	% Organic Matter	% LOI Values	% Carbon
Ferrihydrite + Alginate (M.W.=106.87g/mol)	33.01	30.89	63.11 ± 0.51	36.89 ± 0.51	26.22 ± 0.72	9.38 ± 0.61
Lepidocrocite + Alginate (M.W.= 88.85g/mol)	33.01	37.15	44.78 ± 0.55	55.22 ± 0.55	10.43 ± 0.78	6.11 ± 0.09
Goethite + Alginate (M.W.= 88.85g/mol)	33.01	37.15	43.47 ± 0.7	56.53 ± 0.75	13.06 ± 1.1	7.37 ± 0.06

Loss of ignition (LOI) analysis (Table 3) showed that the addition of alginate increased the percentage of water and organic matter in biogenic ferrihydrite, lepidocrocite, and goethite. This is to be expected with the high carbon content ($C_6H_9NaO_7$) that makes up the exopolysaccharide alginate. The following LOI values for FhA, LepA, and GA were as follows: 26.22±0.72, 10.43±0.78, and 13.06±1.1%., respectively.

3.2. Non-sequential chemical extractions to determine Fe-bearing fractions for Fe $(OH)_3$, γ-FeOOH, and α –FeOOH

Table 4 presents the non-sequential chemical extraction data to determine the amount of iron extracted from each synthetic Fe-oxide. Within all 18 samples, there was no significant differences in the total iron fraction between Fe $(OH)_3$, γ-FeOOH, and α -FeOOH pre and post addition of alginate and when subjected to the two different radiation doses ($p > 0.05$). The majority of the bioavailable iron fraction was determined to be predominantly amorphous with the exception of lepidocrocite and goethite, which was 12% and 23% crystalline, which is expected due to their mineralogical structures. The HCl and ascorbate extraction data were sufficient indicators of amorphous iron within the Fe-oxide samples. It was observed that the oxalate extraction was lower (for all samples) than the HCl and ascorbate extractions, respectively. However, the oxalate extraction did display larger values for the

amorphous fraction than the Fe (II) fraction. The dithionite extraction values for all samples were on average higher than the ascorbate and oxalate extraction values, which indicates it is a good estimator to determine total iron within the samples. This result is comparable to what was found by Kostka and Luther (1994), that the oxalate extraction over estimates the amorphous fraction and underestimates the crystalline iron fraction (Fe (II) catalyzes the dissolution of crystalline Fe-oxides).

Table 4: Non-sequential chemical extraction data of the solid Fe-oxides (Ferrihydrite (Fh), Lepidocrocite, and Goethite) uncertainty with the addition of the EPS alginate and subjected to gamma irradiation.

	Solid Phase Iron (mg/gdwt)- Uncertainty=2SD						Fraction (%)	
Fe-Oxides	**0.5 HCl (H) Fe(II)**	**0.5 HCl (H) Amorphous**	**Ascorbate (A)**	**Oxalate (O) Fe(II)**	**Oxalate (O) Amorphous**	**Dithionite (D)**	**Amorphous[a]**	**Crystalline[b]**
Lep	0.2 ± 0.1	269 ± 83	301 ± 27	3.6 ± 0.8	11 ± 3.3	243 ± 8.0	100 ± 7	0
Lep (5kGy)	0.3 ± 0.4	218 ± 20	288 ± 39	3.8 ± 0.2	11 ± 1.4	233 ± 2.7	100 ± 15	0
Lep (28kGy)	1.7 ± 1.1	274 ± 26	325 ± 3.4	4.0 ± 0.6	14 ± 0.4	299 ± 3.7	100 ± 0.6	0
LepA	13 ± 2.5	2715 ± 317	245 ± 41	7.6 ± 0.9	20 ± 3.4	279 ± 67	88 ± 35	12 ± 35
LepA (5kGy)	4.8 ± 6.4	3211 ± 26	337 ± 64	6.0 ± 2.0	21 ± 6.2	303 ± 24	100 ± 23	0
LepA (28kGy)	22 ± 3.3	3779 ± 711	324 ± 13	10 ± 0.9	20 ± 3.0	370 ± 58	88 ± 17	12 ± 17
G	12 ± 0.4	2622 ± 247	332 ± 13	4.5 ± 0.7	14 ± 0.6	427 ± 25	78 ± 3.0	22 ± 3.0
G (5kGy)	13 ± 0.8	2850 ± 207	386 ± 27	4.4 ± 0.1	13 ± 0.3	519 ± 44	74 ± 9.5	26 ± 9.5
G (28kGy)	11 ± 0.8	3154 ± 136	429 ± 33	4.0 ± 0.2	13 ± 0.9	400 ± 46	100 ± 11	0
GA	14 ± 1.2	3283 ± 41	680 ± 45	8.1 ± 0.9	25 ± 1.7	656 ± 49	100 ± 6.1	0
GA (5kGy)	19 ± 2.9	4300 ± 555	693 ± 64	9.3 ± 0.7	22 ± 1.6	674 ± 51	100 ± 15	0
GA (28kGy)	15 ± 1.7	3457 ± 164	695 ± 19	10 ± 0.6	30 ± 4.4	905 ± 113	77 ± 11	23 ± 11
Fh	55 ± 3.1	20240 ± 614	688 ± 130	13 ± 1.0	47 ± 1.1	709 ± 68	97 ± 8.8	3.0 ± 8.8
Fh (5kGy)	54 ± 0.3	19909 ± 441	643 ± 26	15 ± 1.3	42± 1.6	630 ± 49	100 ± 12.	0
Fh (28kGy)	51 ± 1.3	20652 ± 1056	793 ± 60	16 ± 4.6	46 ± 6.7	625 ± 19	100 ± 10	0
FhA	64 ± 2.4	3793 ± 209	351 ± 35	15 ± 3.0	51 ± 7.8	333 ± 40	100 ± 11	0 ± 11
FhA (5kGy)	58 ± 1.5	8582 ± 219	329 ± 31	15 ± 2.4	61 ± 3.8	380 ± 66	87 ± 18	14 ± 18
FhA (28kGy)	59 ± 4.4	7594 ± 729	303 ± 10	16 ± 1.9	70 ± 7.7	354 ± 24	88 ± 5.8	14 ± 5.8

[a] Amorphous fraction calculated using the equation: (A/D) X 100
[b] Crystalline fraction calculated using the equation: (D-A/D) X 100

3.3 Reduction of Synthetic Fe-Oxides

3.3.1. Ferrihydrite (Fh) and Ferrihydrite + Alginate (FhA)

After 24 hours, in the biotic microcosm, the reduction potential (Eh) for Fh, Fh-5kGy, and Fh-28 kGy decreased rapidly (approximately by 150 mV). The Eh continued to drop for 7 days at which point it achieved a steady state for the remainder of the experiment. The microcosm reduction results for Fh, Fh-5kGy, Fh-28kGy, FhA, FhA-5kGy, and FhA-28kGy are presented in Figure 1^{A-C}. For the duration of each Fh and FhA microcosm experiment (including the irradiated samples), cell counts remained constant within the range of $3.1 \times 10^7 – 8.4 \times 10^7$, respectively. The Fe (III) reduction for ferrihydrite with and without alginate (Figure 1^{A}) was completed by the 17^{th} day with a maximum Fe (III) reduction of 80 and 100%, respectively (Table 5). However, it was observed that the presence of EPS alginate led to a faster reduction rate for ferrihydrite and maximum Fe (III) reduction (100%). The reduction rates for Fh and FhA were 0.057 ± 0.040 and 0.074 ± 0.029 day^{-1} with normal distribution following first order kinetics, respectively. While there was a slightly faster observed reduction rate for FhA than Fh (Table 5), there was no significant difference ($p> 0.05$) for both samples. It must be noted that for all Fh and FhA microcosm experiments, full Fe (III) reduction was achieved by the 17^{th} day (Figure 1^{A-C}).

Ferrihydrite and FhA subjected to gamma irradiation at 5kGy (Figure 1^{B}) and 28kGy (Figure 1^{C}) yielded relatively similar results to the Fh and FhA non-gamma irradiated samples. The Eh values significantly decreased after 24 hours of post-inoculation (by approximately 200 mV) for all four minerals (Figure 1^{B} and Figure 1^{C}) and continued to decline for 7 days of post-inoculation at which point steady state was achieved for the remainder of the experiment. The cell counts for all microcosm experiments ranged between 1.0×10^7-1.4×10^8. The Fe (III) reduction for Fh and FhA irradiated at 5kGy (Figure 1^{B}) was similar to that of Fh and FhA (non-gamma) (Table 5), achieving rates of 0.037 ± 0.012 and 0.041 ± 0.015 and reaching maxima of 62 and 80% Fe (III) reduction with no significant difference ($p> 0.05$).

The reduction of ferrihydrite and ferrihydrite with alginate irradiated at 28kGy (Figure 1^{C}) was observed to have slightly higher reduction rates (0.043 ± 0.015 and 0.059 ± 0.032 day^{-1}) when compared to Fh-5kGy and FhA-5kGy irradiated but slower than the non-gamma irradiated samples of Fh and FhA. The maximum Fe (III) reduction achieved over a 17 day period was determined to be 65% for Fh-28kGy and 84% for FhA-28kGy. However, there was no significant difference between the two samples ($p > 0.05$). It was observed that for all ferrihydrite-alginate minerals (gamma irradiated and non-gamma inclusive), that the exopolysaccharide promoted increased Fe (III) reduction rates and percentage of total iron reduced while gamma irradiation had no significant effect on the Fh and FhA (gamma irradiated and non-gamma inclusive).

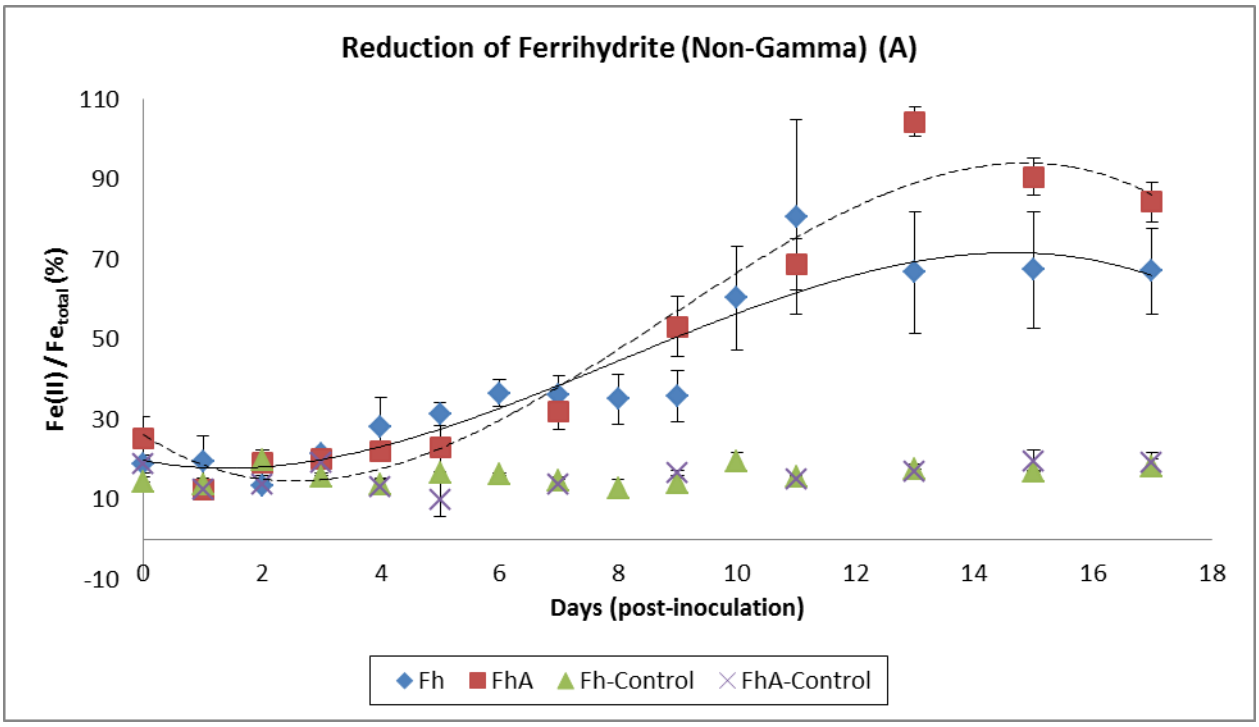
Reduction of Ferrihydrite (Non-Gamma) (A)
Fe(II) / Fe$_{total}$ (%)
110
90
70
50
30
10
-10
0
2
4
6
8
10
12
14
16
18
Days (post-inoculation)
Fh
FhA
Fh-Control
FhA-Control

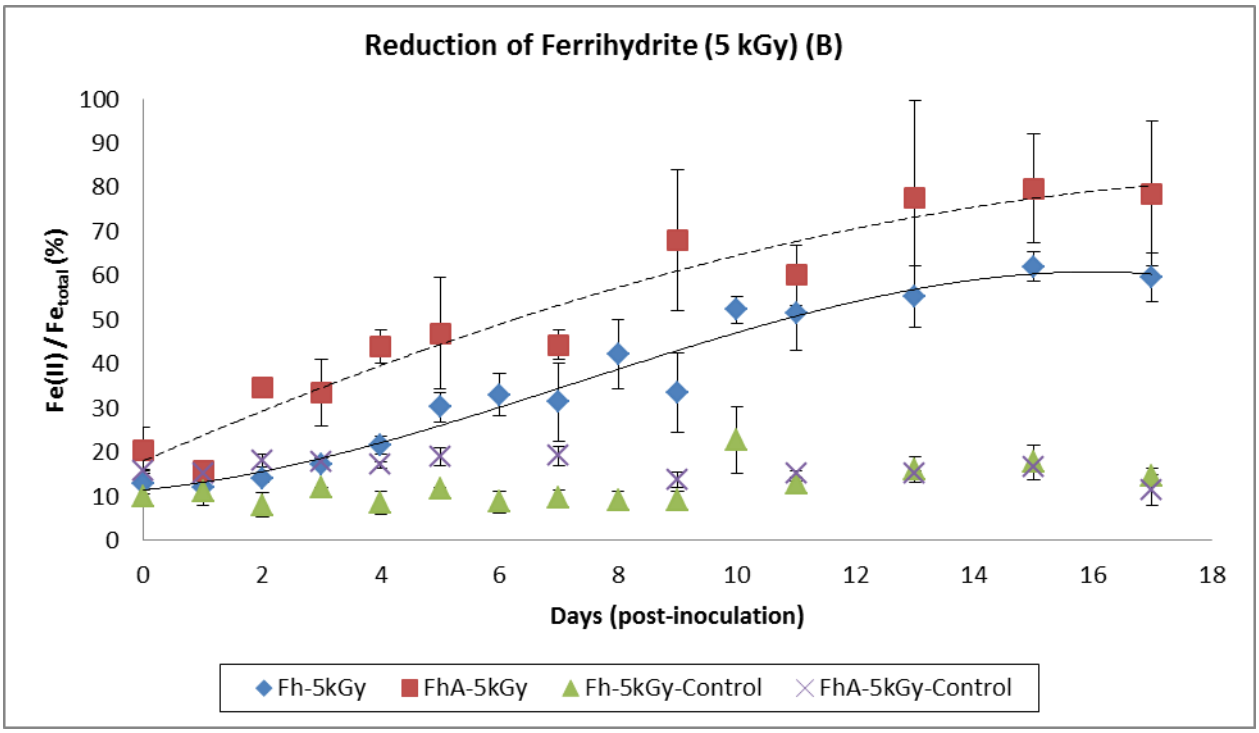
Reduction of Ferrihydrite (5 kGy) (B)
Fe(II) / Fe$_{total}$ (%)
100
90
80
70
60
50
40
30
20
10
0
0
2
4
6
8
10
12
14
16
18
Days (post-inoculation)
Fh-5kGy
FhA-5kGy
Fh-5kGy-Control
FhA-5kGy-Control

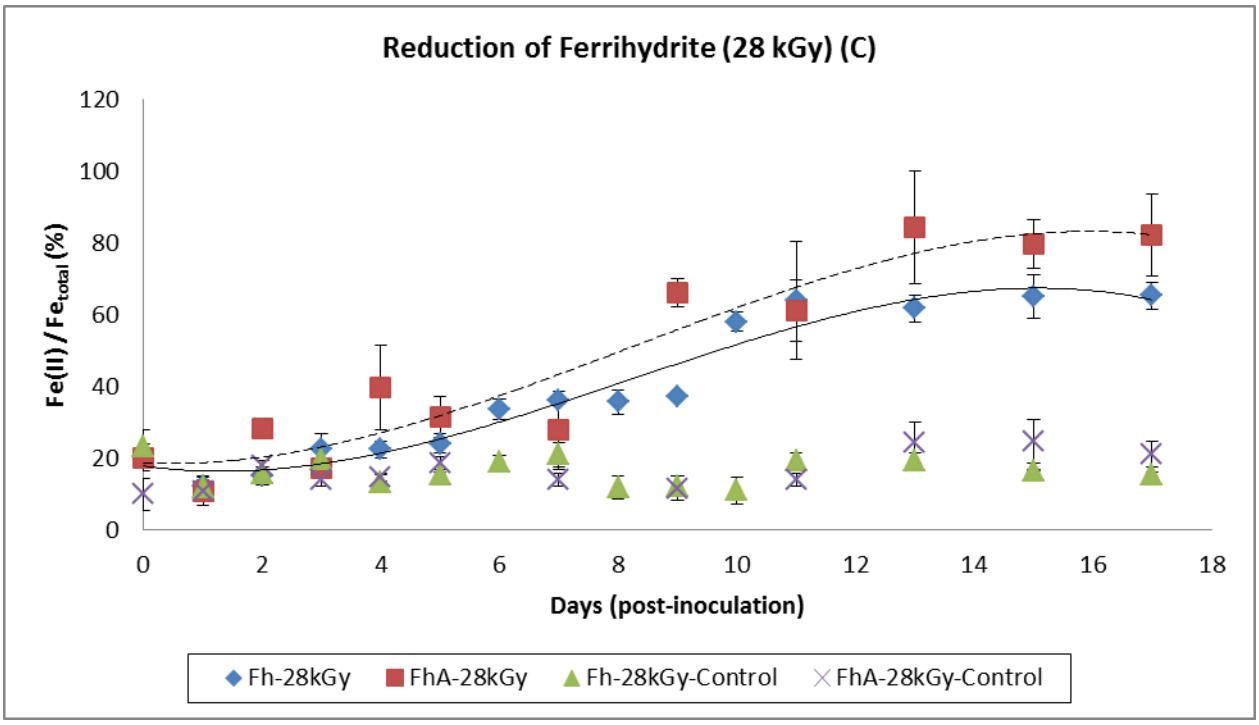

Figure 1: Changes of total Fe (II)/total Fe ratios during the reduction of (A) Ferrihydrite (Fh) and Ferrihydrite + Alginate (FhA) and Fh and FhA subjected to sterilization using gamma irradiation at (B) 5kGy and (C) 28 kGy by *S. putrefaciens* CN32. Data markers represent means and standard deviations of 3 replicate experiments. Solid lines represent 3-parameter sigmoid lines of best fit to the data for Fh data and the dashed lines represent 3-parameter sigmoid lines of best fit to the data for FhA. Respective abiotic (control) experiments are included within the figures. Correlation coefficient (R^2) of the fitted lines are (A) Fh=0.719, FhA=0.899, (B) Fh=0.917, FhA=0.904, and (C) Fh=0.907, FhA=0.821.

3.3.2. Lepidocrocite (Lep) and Lepidocrocite + Alginate (LepA)

The Fe (III) reduction of lepidocrocite (non-gamma) and lepidocrocite with alginate was observed to achieve maximum reduction (79 and 46%) over the duration of 27 and 21 days at a rate of 0.029 ± 0.019 and 0.035 ± 0.031, respectively (Figure 2^{A}) (Table 5). The Eh of both microcosms decreased significantly in the first 4 days (approximately 220 mV) at which point steady state was achieved for the remainder of the experiments. The initial reduction of Lep and LepA coincided with the decrease in the proportion of Fe (II)/Fe (III) however, LepA reached a maximum over a shorter period while Lep continued to be reduced. The cell count for each of the iron minerals remained high for the first 5 days of the experiments (5.2×10^7 and 4.6×10^7 CFU/mL) at which point there was a notable decline in the

LepA cell count to 3.1 x 10^5 CFU/mL. The decline in bacteria can be attributed to the lower proportion of Fe (II)/Fe (III) throughout the LepA experiment, which as can be observed in Figure 2^A after day 7, where the percentage of total reduced iron decreased and reached a steady state.

The gamma irradiated (5kGy and 28kGy) lepidocrocite and lepidocrocite with alginate samples followed similar trends, achieving faster Fe (III) reduction rates and higher total reduced iron percentages than the samples that were not gamma irradiated. Figure 2^B displays the iron reduction experiment for Lep and LepA gamma irradiated at 5kGy. The proportion of Fe (II) /Fe (III) for Lep-5kGy and LepA-5kGy were similar from day 0 to day 5, however on day seven, there was an increase in total Fe (III) reduction (58%) at which point the rate of reduction decreased until day 15, where maximum reduced total iron reached 80%. The rate of reduction for Lep-5kGy and LepA-5kGy gamma was 0.014 ± 0.012 and 0.039 ± 0.031 day^{-1}, respectively. There was a significant difference between Lep-5kGy and LepA-5kGy ($p < 0.05$) and as mentioned, this difference can be attributed to the decrease in *S. putrefaciens* cell count throughout each experiment with cell counts reaching 1.8 x 10^8 and 1.0 x 10^7 in the Lep-5kGy and LepA-5kGy, respectively.

Lepidocrocite and lepidocrocite with alginate samples gamma irradiated at 28kGy (Figure 2^C) behaved similarly to the 5kGy samples (Figure 2^B). The Eh values for both Lep-28kGy and LepA-28kGy decreased rapidly over the first 24 hours post-inoculation (51 mV and 150 mV) at which point the Eh values for both minerals continued to decrease but reached a steady state at approximately 150mV and 200mV (day 3 post-inoculation) for the remainder of the experiment. Figure 2^C displays the percentage of total iron reduced for Lep-28kGy and LepA-28kGy to be similar for the first 5 days post-inoculation and at day 7, the percentage of total iron reduced for LepA-28kGy increased to 36% on day 5 and continued to increase until a maximum of 72% was attained on day 13, while Lep-28kGy reached the maximum of 51% of total reduced iron on day 11 and remained within the standard deviation (Table 5) for the remainder of the reduction. The rates of reduction observed for Lep-28kGy and LepA-28kGy

were comparable to those of the 5kGy samples at 0.02 ± 0.020 and 0.039 ± 0.027 day^{-1}, respectively. There was no significant difference in the percent of total iron reduced between Lep-28kGy and LepA-28kGy ($p > 0.05$) and no indication that gamma radiation affected the mineralogical properties (confirmed by XRD) (Appendix H) or the microbial reduction of Lep-28kGy and LepA-28kGy.

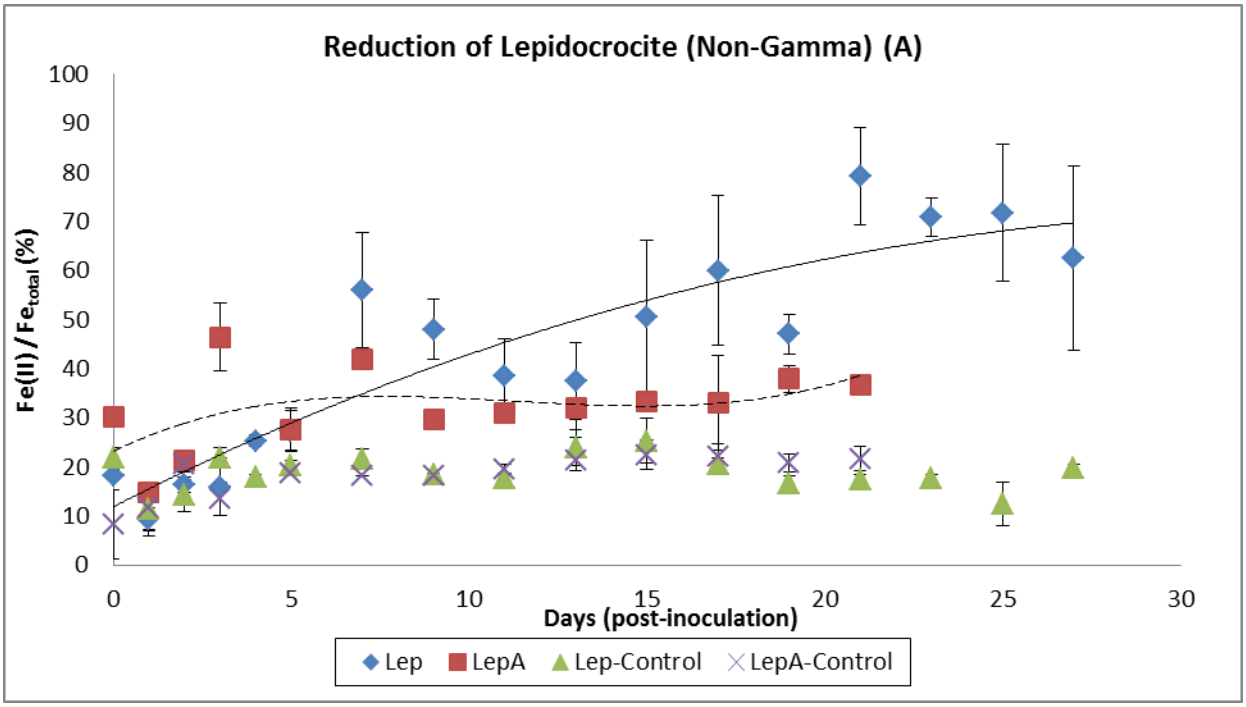
Reduction of Lepidocrocite (Non-Gamma) (A)
Fe(II) / Fe total (%)
Days (post-inoculation)
Lep
LepA
Lep-Control
LepA-Control

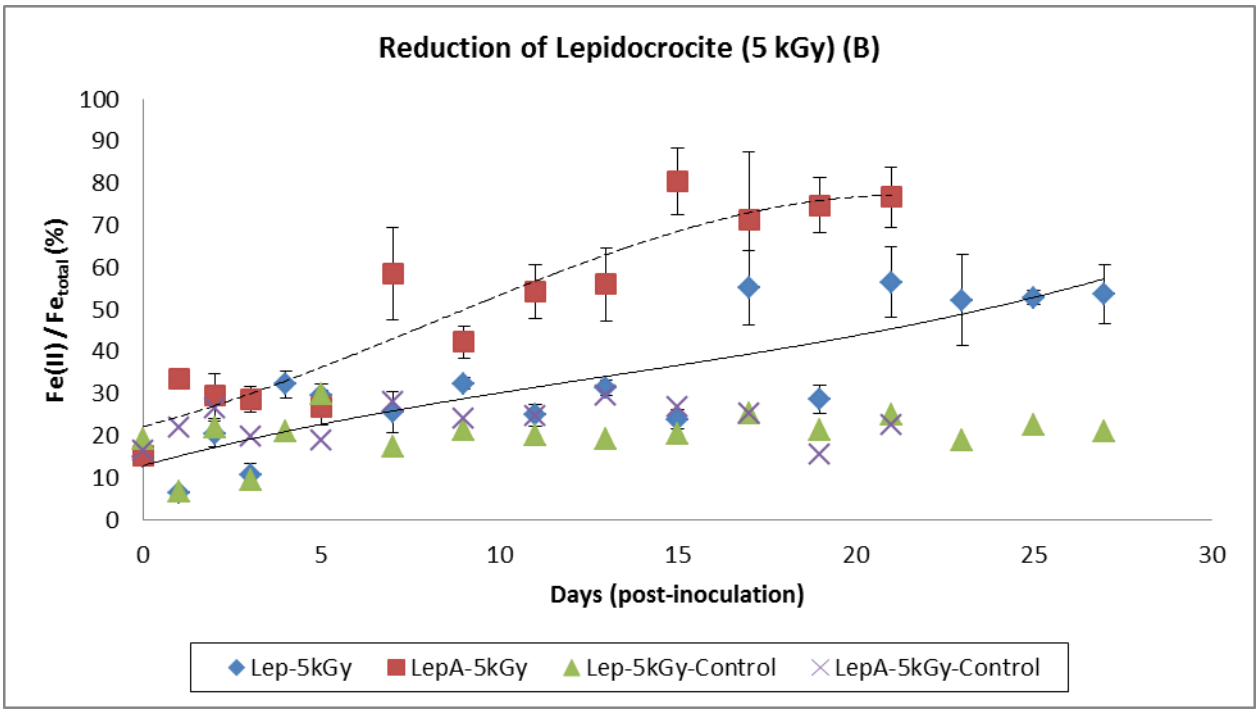
Reduction of Lepidocrocite (5 kGy) (B)
Fe(II) / Fe total (%)
Days (post-inoculation)
Lep-5kGy
LepA-5kGy
Lep-5kGy-Control
LepA-5kGy-Control

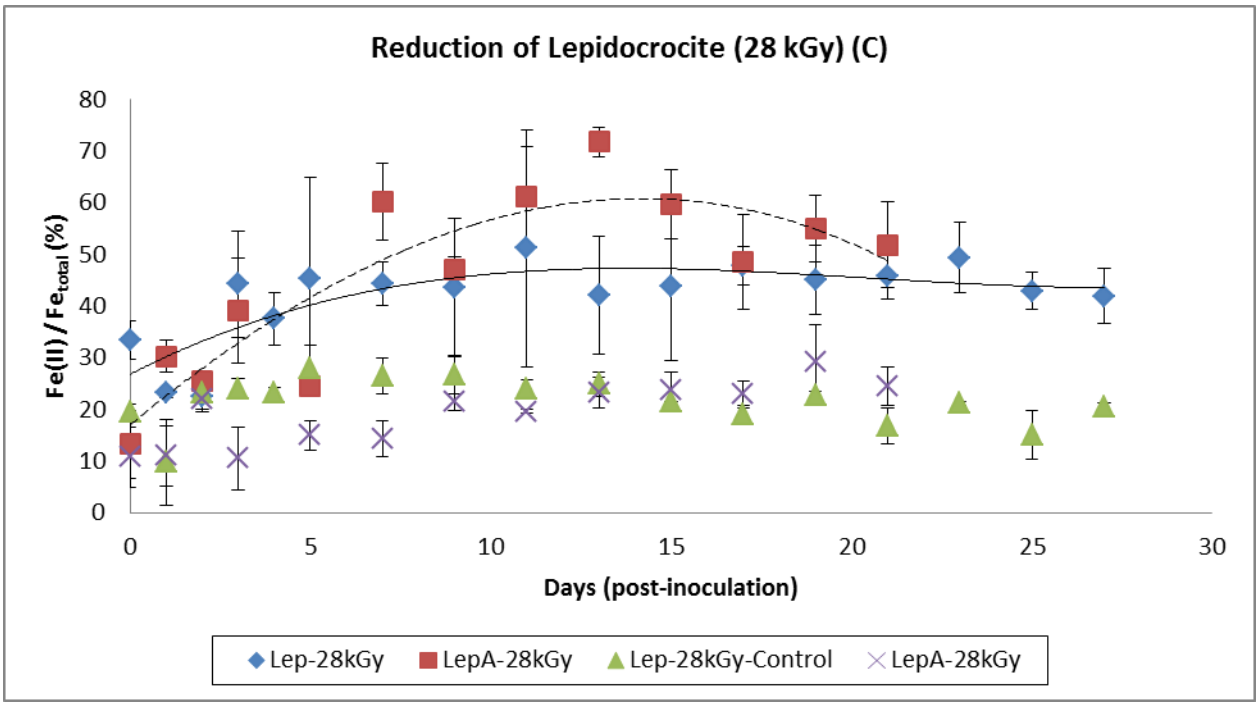

Figure 2: Changes of total Fe (II)/total Fe ratios during the reduction of (A) Lepidocrocite (Lep) and Lepidocrocite + Alginate (LepA) and Lep and LepA subjected to sterilization using gamma irradiation at (B) 5kGy and (C) 28 kGy by *S. putrefaciens* CN32. Data markers represent means and standard deviations of 3 replicate experiments. Solid lines represent 3-parameter sigmoid lines of best fit to the data for Lep data and the dashed lines represent 3-parameter sigmoid lines of best fit to the data for LepA. Respective abiotic (control) experiments are included within the figures. Correlation coefficient (R^2) of the fitted lines are (A) Lep=0.632, LepA =0.392, (B) Lep=0.348, LepA =0.667, and (C) Lep=0.51, LepA =0.743.

3.3.3. Goethite (G) and Goethite + Alginate (GA)

The duration of the microcosm experiments for goethite (G) and goethite with alginate (GA) (Figure 3^{A}) spanned over a period of 28 and 21 days, respectively. High reduction of Fe (III) was observed for both samples with the maximum percentage of total iron reduced determined to be 91% for goethite and 100% for GA (Figure 3^{A}), which suggests full reduction of Fe (III). Cell counts remained high for the duration of the experiment until maximum iron reduction was reached, at which point the cell counts decreased, the observed cell count range for goethite was determined to be $2.8 \times 10^8 – 2.7 \times 10^7$ CFU/mL and $3.3 \times 10^8 – 2.7 \times 10^7$ CFU/mL for GA. The rate of reduction for G and GA was relatively similar to the reduction rates of ferrihydrite and lepidocrocite with the observed rates being 0.045 ±

0.010 and 0.048 ± 0.022 day^{-1} (Table 5), respectively. However, the reduction of GA began rapidly and reached approximately 65% of total reduced iron at which point reduction slowed down to day 8 where the percentage of total iron increased approximately to 20%. The rapid reduction of GA corresponded to the rapid decline in the Eh value, which declined by approximately 200mV in the first 24 hours. A lower Eh decline was observed for goethite (Figure 3^{A}), i.e., approximately 60mv in 24 hours. Within the first 72 hours, the percent of total iron reduced was 20% and remained relatively low until day 13 where the percentage increased approximately to 50%. A significant difference between the rates of reduction for goethite and goethite with alginate was noted ($p < 0.05$), which is also indicated by the percentage of total iron reduced as displayed in Figure 3^{A}.

Figure 3^{B} and 3^{C} display the reductions of G and GA gamma irradiated samples at 5 and 28kGy. Results indicate that gamma radiation (0, 5, and 28kGy) does not affect Fe (III) reduction as confirmed by XRD and the reduction of G and GA in Figure 3^{A}. GA-5kGy underwent a faster rate of reduction (x2) than G-5kGy (Table 5). The Fe (III) reduction rates of G-5kGy and GA-5kGy were 0.023 ± 0.010 and 0.052 ± 0.029 day^{-1}, respectively. Full Fe (III) reduction (100%) of GA-5kGy was observed after 18 days of post-inoculation while 70% was observed after twenty-five days of post-inoculation for G-5kGy. There was a significant difference between G-5kGy and GA-5kGy ($p < 0.05$). The trend observed for the first 5 days post-inoculation for GA-5kGy exhibited a rapid increase in Fe (III) reduction (approximately 50%) and then declined on day 6, at which point a trend of increased Fe (III) reduction followed by a decrease in Fe(III) reduction occurred every 24 hours until day 10. The Eh values followed the same trend where there was a continuous decrease until the steady state was reached at day 5 (≈-240mV) and for the remainder of the experiment. This is indicative of a decrease in the number of cells of *S. putrefaciens* CN32 from day 0 to day 6 (3.3×10^{8} to 7.3×10^{7} CFU/mL). The G-5kGy total iron reduction was much slower than GA-5kGy and displayed a slower decline in the number of *S. putrefaciens* CN32 cells.

The reduction results for G-28kGy and GA-28kGy (Figure 3^{C}) were significantly different ($p < 0.05$) but exhibits similar trends to those of G-5kGy and GA-5kGy. Goethite-28kGy underwent a slower Fe (III) reduction (0.025 ± 0.020 day^{-1}), achieving maximum percent total iron reduction at 54% over the 28day microcosm experiment. The Eh declined very slowly over the first 24 hours (30mV) and then rapidly to reach approximately -160mV, which can be attributed to *S. putrefaciens* adjusting to the anaerobic conditions of the chemically defined medium (CDM). The cell counts for the G-28kGy experiment was on average around 6.4×10^{7} CFU/mL. The microcosm experiment for GA-28kGy displayed the same trend of rapid Fe (III) reduction over the first 5 days of post-inoculation (≈ 70% total reduced iron). On day 6, reduction slowed down followed by a rapid reduction until day 11 which reached a maximum total reduced iron of 96% after 22 days of post-inoculation with a reduction rate of 0.039 ± 0.033 day^{-1}.

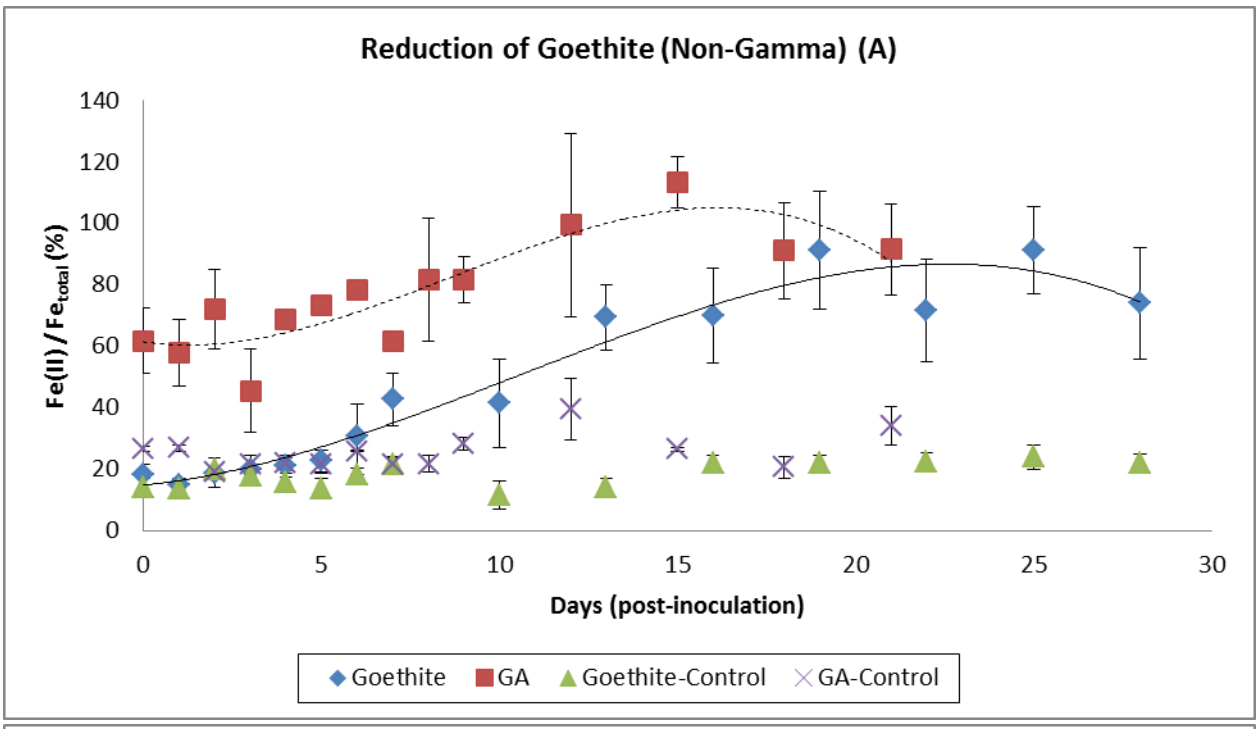
Reduction of Goethite (Non-Gamma) (A)
Fe(II) / Fe$_{total}$ (%)
140
120
100
80
60
40
20
0
0
5
10
15
20
25
30
Days (post-inoculation)
Goethite
GA
Goethite-Control
GA-Control

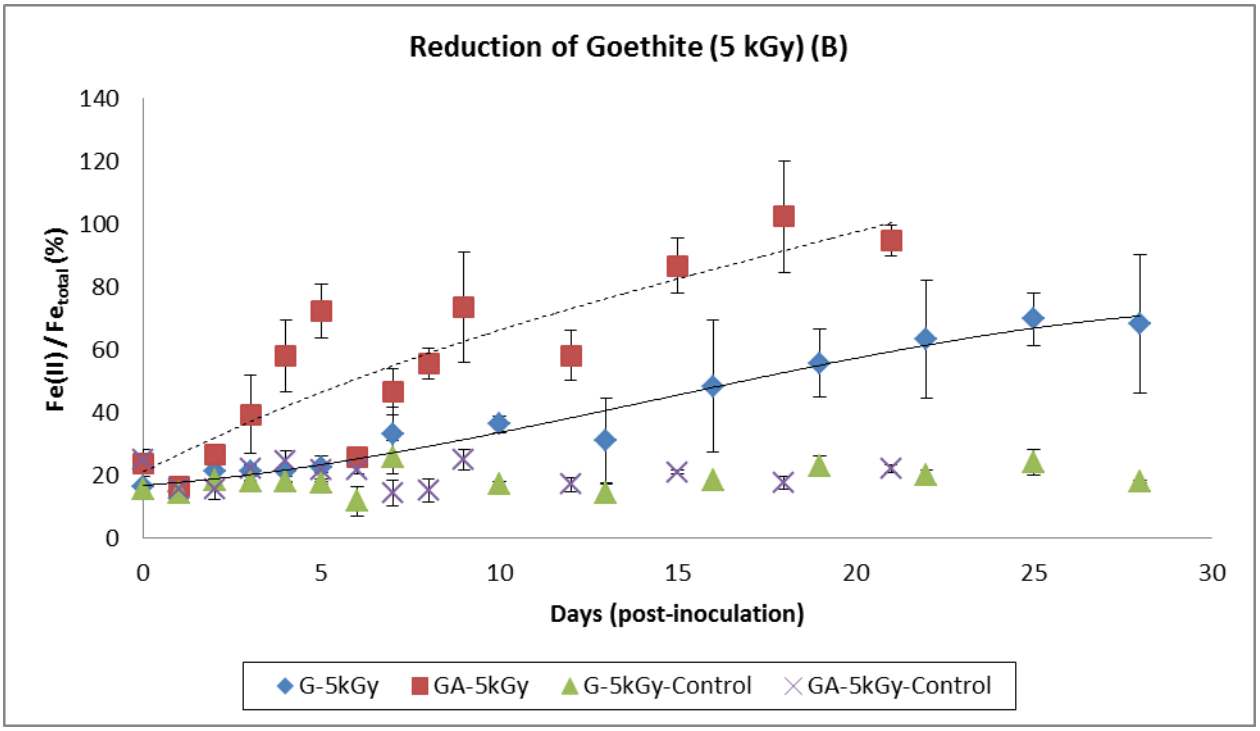
Reduction of Goethite (5 kGy) (B)
Fe(II) / Fe$_{total}$ (%)
140
120
100
80
60
40
20
0
0
5
10
15
20
25
30
Days (post-inoculation)
G-5kGy
GA-5kGy
G-5kGy-Control
GA-5kGy-Control

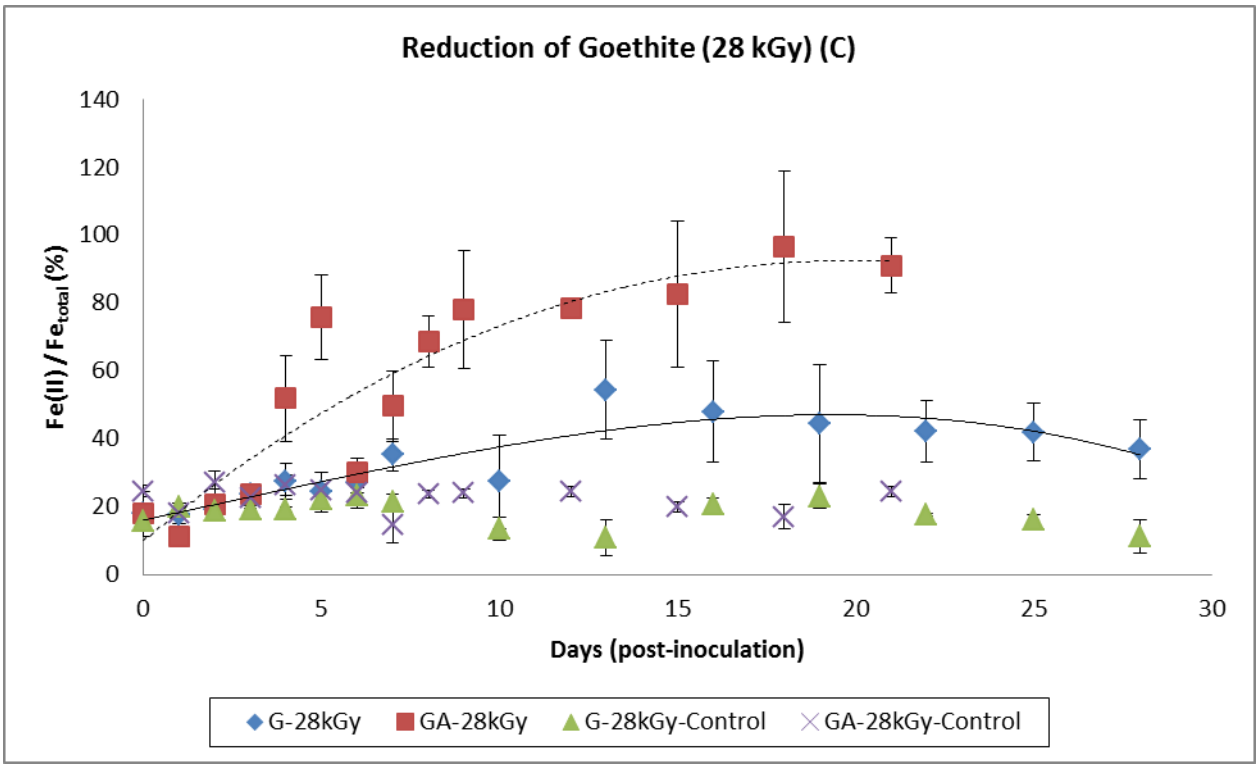

Figure 3: Changes of total Fe (II)/total Fe ratios during the reduction of (A) Goethite (G) and Goethite+ Alginate (GA) and G and GA subjected to sterilization using gamma irradiation at (B) 5kGy and (C) 28 kGy by *S. putrefaciens* CN32. Data markers represent means and standard deviations of 3 replicate experiments. Solid lines represent 3-parameter sigmoid lines of best fit to the data for G data and the dashed lines represent 3-parameter sigmoid lines of best fit to the data for GA. Respective abiotic (control) experiments are included within the figures. Correlation coefficient (R^2) of the fitted lines are (A) G=0.959, GA =0.846, (B) G=0.949, GA =0.818, and (C) G=0.663, GA =0.546.

3.4 Rates of Fe (III) Reduction for the Fe-Oxide Minerals Fh, FhA, Lep, LepA, G, and GA

Total Fe (III) reduction rates were calculated from the total Fe (II)/total Fe (III) proportions determined from the microcosm experiments using the minimum to maximum range of proportions and plotted against time (days post inoculation). The reduction rates (day^{-1}) for all 18 Fe-oxide samples are presented in Table 5. Based on statistical analysis, all samples containing alginate had faster reduction rates (day^{-1}) than samples without it. Ferrihydrite underwent faster Fe (III) reduction than lepidocrocite and goethite, respectively. The pH for all samples during the reduction experiments was observed to range within 6.73-7.55. For the majority of the experiment, the pH remained near neutrality, however

after the maximum total reduced iron was achieved and the reduction rate slowed down, the pH slightly increased (pH > 7.15).

Table 5: Fe (III) Reduction Rates and Total Reduced Iron for Ferrihydrite, Lepidocrocite, and Goethite (No Radiation, Gamma Radiation at 5 and 28 kGy, and the addition of Alginate inclusive).

Fe-Oxide	Maximum % Total Fe Reached	Reduction Rate (day^{-1})	R^2
Ferrihydrite (Non-Gamma)	80.55 ± 0.24	0.057 ± 0.040	0.719
Ferrihydrite (5 kGy)	62.02 ± 0.03	0.037 ± 0.012	0.917
Ferrihydrite (28 kGy)	65.29 ± 0.03	0.043 ± 0.015	0.907
Ferrihydrite + Alginate (Non-Gamma)	104.3 ± 0.04	0.074 ± 0.029	0.899
Ferrihydrite + Alginate (5 kGy)	79.7 ± 0.12	0.041 ± 0.015	0.904
Ferrihydrite + Alginate (28 kGy)	84.35 ± 0.16	0.059 ± 0.032	0.821
Lepidocrocite (Non-Gamma)	79.15 ± 0.10	0.029 ± 0.019	0.632
Lepidocrocite (5 kGy)	56.48 ± 0.08	0.014 ± 0.012	0.348
Lepidocrocite (28 kGy)	51.15 ± 0.23	0.020 ± 0.020	0.51
Lepidocrocite + Alginate (Non-Gamma)	46.39 ± 0.07	0.035 ± 0.051	0.392
Lepidocrocite + Alginate (5 kGy)	80.37 ± 0.08	0.039 ± 0.031	0.667
Lepidocrocite + Alginate (28 kGy)	71.7 ± 0.03	0.039 ± 0.027	0.743
Goethite (Non-Gamma)	91.17 ± 0.19	0.045 ± 0.010	0.959
Goethite (5 kGy)	69.71 ± 0.08	0.023 ± 0.010	0.949
Goethite (28 kGy)	54.35 ± 0.15	0.025 ± 0.020	0.663
Goethite + Alginate (Non-Gamma)	103.3 ± 0.08	0.048 ± 0.022	0.846
Goethite + Alginate (5 kGy)	102.28 ± 0.18	0.052 ± 0.029	0.818
Goethite + Alginate (28 kGy)	96.45 ± 0.22	0.039 ± 0.033	0.546

3.5. Post-Reduction Minerology and Quality Control Experiments (i.e., sunlight exposure, use of ferric nitrate salts and age of the inoculum)

The post- reduction mineralogy (determined by XRD) of the secondary minerals in the ferrihydrite (Fh and FhA), lepidocrocite (Lep and LepA), and goethite (G and GA) microcosms is presented in Appendix A (A-4 to A-6). It was determined that vivianite ($Fe_3(PO_4)_2 \cdot 8H_2O$) formed in all of the biotic microcosm experiments. The secondary mineral, vivianite, has been previously observed (Langley et al., 2009[B] and Najem et al., 2016) in chemically defined media with high concentrations of phosphate (3.9 and 4.0mM). There were no mineralogical changes to the abiotic microcosms.

The Fe (III) rates of reduction of all ferrihydrite samples synthesized with a ferric nitrate salt solution (Table 5) were compared to those synthesized using a ferric chloride salt solution (Table 6). Results indicate no significant differences ($p > 0.05$). The results include all ferrihydrite samples synthesized with the addition of alginate and gamma irradiated at 5 and 28kGy (Appendix C). The Fe (III) reduction rates of ferrihydrite exposed to sunlight versus ferrihydrite protected from direct sunlight was 0.068 ± 0.018 and 0.050 ± 0.020 day^{-1} (Table 6), respectively. While it is observed, in Figure 4^{A} that ferrihydrite in the presence of sunlight undergoes a faster reduction rates, similar maximum total reduced iron percentages were reached for the Fh and FhA (0kGy) experiments (Figure 1^{A}) (Table 5) and there was no significant difference ($p > 0.05$) between the Fe (III) reduction rates of ferrihydrite in the presence of sunlight versus protected from sunlight. It should also be noted that sunlight had no effect on the use of different ferric salt solutions during the synthesis as there was no significant difference ($p > 0.05$) observed. The Fe (III) reduction experiments for ferrihydrite using aged and freshly inoculum are presented in Figure 4^{B}. It was observed that both experiments had similar total iron reduction trends with Fe (III) reduction rates for ferrihydrite using aged *S. putrefaciens* and freshly inoculated *S. putrefaciens* determined to be 0.052 ± 0.049 and 0.068 ± 0.039 day^{-1}, respectively and achieving 67 and 70% of maximum total reduced iron (Table 5). There was no significant difference ($p > 0.05$) between the total iron (III) reduction experiments for ferrihydrite using aged versus freshly inoculation *S. putrefaciens* with respect to reduction rates.

Table 6: Reduction Rates of Ferrihydrite tested using aged and new CN32 while in the presence of sunlight (No Radiation, Gamma Radiation at 5 and 28 kGy, and the addition of Alginate).

Fe-Oxide*	Maximum % Fe Reached	Linear Reduction Rate (day−1[a])	R^2
Ferrihydrite (Non-Gamma)	85.28 ± 0.04	0.072 ± 0.010	0.986
Ferrihydrite (5 kGy)	77.36 ± 0.09	0.057 ± 0.012	0.965
Ferrihydrite (28 kGy)	74.36 ± 0.13	0.045 ± 0.016	0.916
Ferrihydrite + Alginate (Non-Gamma)	62.84 ± 0.09	0.065 ± 0.020	0.943
Ferrihydrite + Alginate (5 kGy)	66.81 ± 0.09	0.038 ± 0.011	0.962
Ferrihydrite + Alginate (28 kGy)	68.16 ± 0.04	0.051± 0.034	0.911
No Light Induced Reduction (Foil)	62.76 ± 0.05	0.05 ± 0.020	0.9
Light Induced Reduction (No Foil)	64.71 ± 0.11	0.068 ± 0.018	0.963
Aged Bacteria (1 week)	66.76 ± 0.15	0.052 ± 0.049	0.613
Fresh Bacteria	70.16 ± 0.04	0.068 ± 0.039	0.856

*Denotes that Fh and FhA samples were synthesized using a Ferric Nitrate Salt compared to Fh and FhA samples outlined in Table 5 where Fh and FhA were synthesized using a ferric nitrate salt.

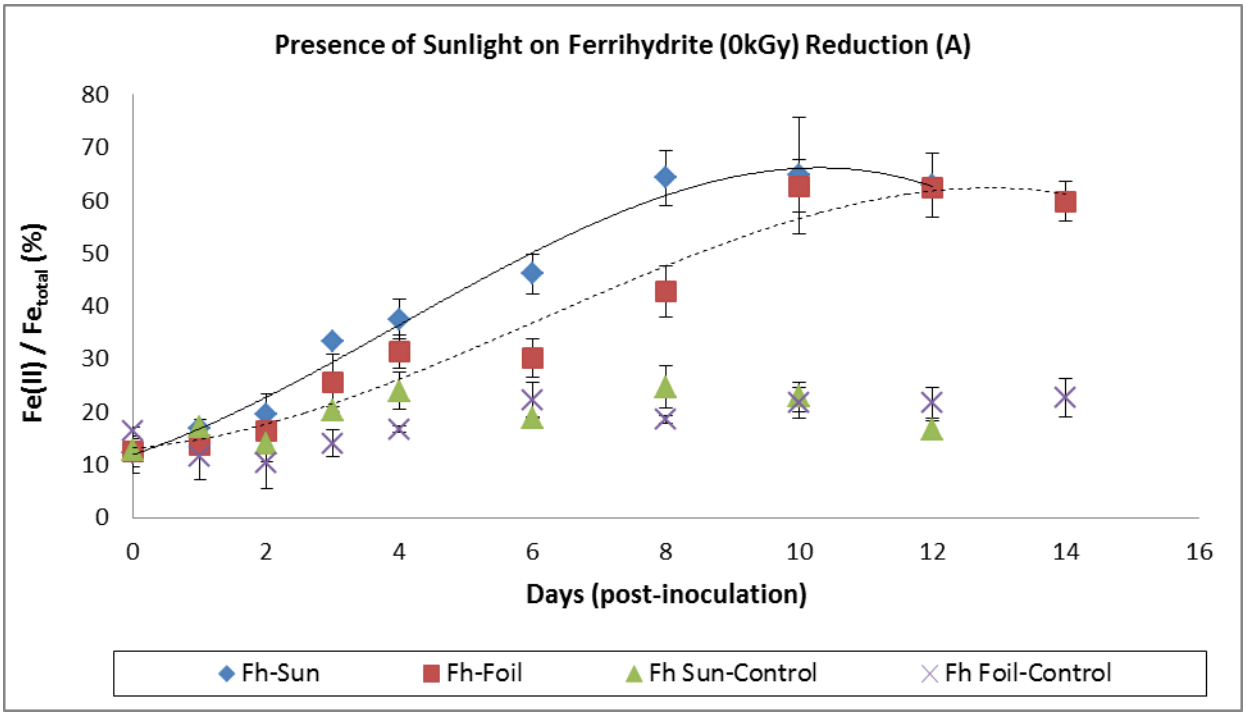

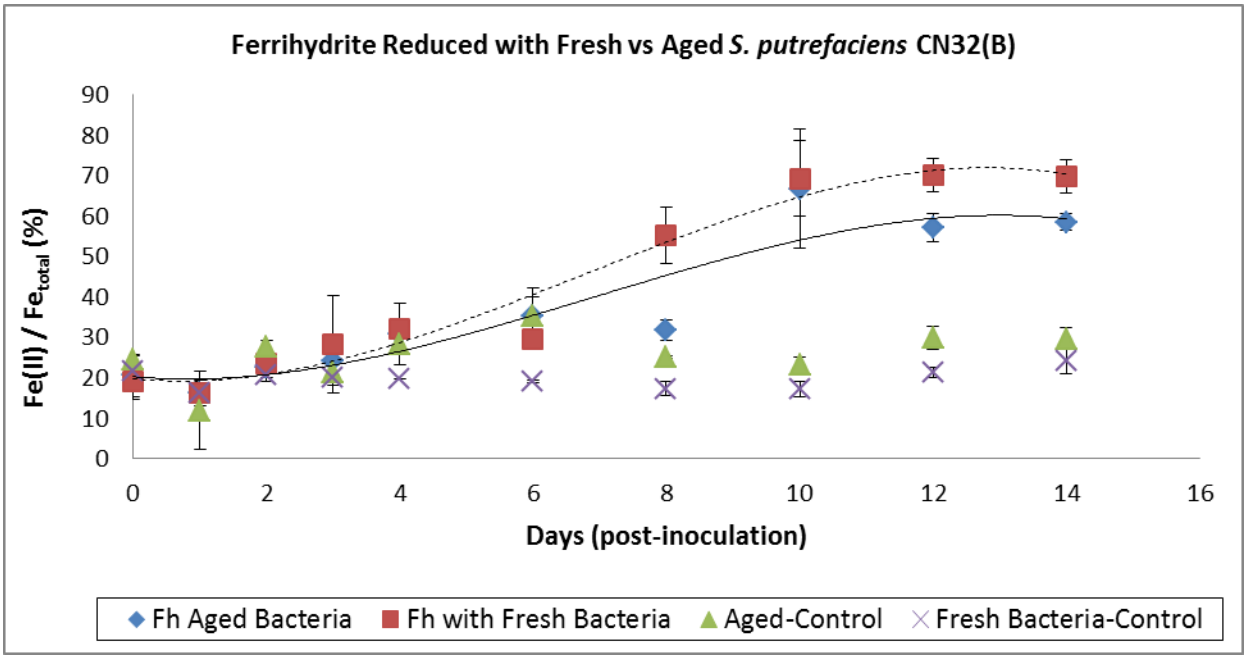

Figure 4: Quality control experiments testing the effects of sunlight and aged versus fresh inoculum of *S. putrefaciens* on the Fe (III) reduction experiments for ferrihydrite. Figure 5 (A) displays the changes to total Fe (II)/total Fe during the reduction of Ferrihydrite (Fh) using *S. putrefaciens* CN32 in the presence of sunlight compared to no sunlight, (B) under the microbial reduction of aged versus fresh inoculum. Data markers represent means and standard deviations of 3 replicate experiments. Solid lines represent 3-parameter sigmoid lines of best fit to the data for Fh data and the dashed lines represent 3-parameter sigmoid lines of best fit to the data for FhA. Respective abiotic (control) experiments are included within the figures. Correlation coefficient (R^2) of the fitted lines are (A) Fh-Sun=0.963, Fh-Foil=0.960 and (B) Fh-Aged=0.613, Fh-Fresh=0.856.

4. Discussion

4.1. Mineralogical Characterization of Synthetic BIOS and Effects of Gamma (γ-) Sterilization

The synthesis of ferrihydrite, lepidocrocite, and goethite via wet chemistry methods outlined in Cornell and Schwertmann (2000) was modified to adjust for the addition of the exopolysaccharide alginate in order to mimic the composition of natural biogenic iron oxides (BIOS), which contain bacterial exopolysaccharides (EPS) and iron oxides (Mikutta, 2008). Due to the number of synthesis pathways in which Fe-oxides and hydroxides can be produced, it is possible to cause changes in specific properties, such as crystal morphology, surface area, crystallinity, and water content (Cornell and Schwertmann, 2000). Ferrihydrite, lepidocrocite, and goethite were synthesized using slightly different methods to ensure that the proper final minerology of the Fe-oxides was achieved. Two-line ferrihydrite was prepared using rapid hydrolysis upon the addition of a Fe (III) salt solution, while goethite and lepidocrocite were subjected to oxidation/hydrolysis to ensure the minerology had lower crystallinity and surface area to better represent natural Fe-oxides (Cornell and Schwertmann, 2000; Glasauer *et al*, 2003). Constraints within the synthesis of the Fe-oxides for this study included the duration of hydrolysis for ferrihydrite (occurrence of longer hydrolysis and fluctuation in pH (i.e., pH>8 will favour goethite)), maintaining the pH and extended oxidation are crucial for the production of lepidocrocite to ensure ferrihydrite is not formed, and while goethite is easily obtained over a wide temperature gradient, there is variation in both the crystal size and shape along with the surface area (Cornell and Schwertmann, 2000; Frankel *et al*, 2016).

The dose rate that the Fe-oxide samples were subjected to in the gamma irradiator was determined using Fricke dosimetry, which is the most well studied and widely used method for the measured ration of Fe (III) for ^{60}Co γ-rays (Klassen *et al*, 1999). Following this procedure, using the equation below, the length of time (hr) in which the sample must remain within the gamma cell to achieve the desired dosage (5kGy and 28kGy for this study.) was determined.

$$\text{Irradiation Time (hr)} = \frac{\text{Dose Rate (kGy/hr)}}{\text{Desired Dose (kGy)}}$$

The irradiator used for the Fe-oxide samples delivers a dosage of roughly 0.8-1.0 kGy/hour, depending on the orientation and size of the samples. This means that in order to achieve 5kGy and 28kGy, the sample would have to be irradiated for a period of 10 and 33 hours for 5kGy and 28kGy, respectively. With the half-life of ^{60}Co being on the on the order of 5 years, it was anticipated that the dose rate will not change considerably over the higher range of gamma irradiation, meaning that in order to achieve 28kGy over the 33 hour period, the dose rate was considered to be constant at 0.8-1.0 kGy/hour. The dose rate based on the amount of time that passed since the initial dosimetry was corrected according to the decay curve of ^{60}Co.

Among the wide range of sterilization techniques, gamma (γ-) sterilization has proven to be the most ideal, meaning it is an effective sterilizing procedure that achieves complete removal of microorganisms without adversely affecting the samples of interest (McNamara *et al*, 2003; Bank *et al*, 2008; Schaller *et* al, 2011; Brown *et al*, 2014). The higher end (28kGy) of the optimum dosage range for this study exceeds the average routine optimum dosage level (25kGy) that is used by physical scientists along with the medical and food industries (Chambers and Attiwill, 1994; McNamara *et al*, 2003). According to the classical XRD technique for the analysis of Fe-oxides (Appendix A), the dosage of gamma irradiation applied to ferrihydrite, lepidocrocite, and goethite did not cause any mineralogical changes as suggested by McNamara *et al* (2003) when compared to the x-ray diffractograms produced by Cornell and Schwertmann (2003).

To further validate the non-adverse effect of gamma radiation on the mineralogy of ferrihydrite, Mossbauer spectroscopy was performed on a few selected samples (Fh, Fh-28kGy, FhA, and FhA-28kGy), for the purpose of quality control, for the identification of the Fe-oxide phases. Mossbauer is a mode of analysis that relies on the nuclear decay of $^{57\text{-}60}$Co isotope to ^{57}Fe by the release of gamma rays

(O'Connor, 1968; Vandegrift and Fultz, 1998). For the purpose of this study Fh, Fh-28kGy, FhA, and FhA-28kGy were analyzed to be one doublet and it was concluded that the iron species were ferrihydrite (Appendix F), with spectra identical to those obtained for ferrihydrite by Cornell and Schwertmann (2003). Samples were run at 293 K and 78 K and differences in the isomer shift (difference in *s* electron density between the source and the absorber) were observed due to the second doppler shift with values of 0.350 and 0.462 mm/s, respectively. The value of 0.350 mm/s indicates a high spin Fe (III) oxygen-coordinated species in octhedral symmetry, which is in aggreement with Cornell and Schwertmann (2003).

The use of Mossbauer spectroscopy at different temperature gradients allows for iron atoms of different oxidation states to absorb at different diagnostic energies and the magnitude of variation within the Fe-oxide mineral composition, which can only be attributed to the presence of Fe (III) in Fh, Fh-28kGy, FhA, and FhA-28kGy when they were analyzed at 293 K and 78 K. The use of alginate during the synthesis of ferrihydrite represented a potential source of radicals capable of reducing Fe (III) during the radiation process, as shown in the following reaction (where R-C-COO^- is alginate anion):

$$\text{R-C-COO}^- + \text{Gammma-Ray} \rightarrow \text{R-C}\cdot + \bullet\text{COO}^- \quad (1)$$

$$\bullet\text{COO}^- \rightarrow \text{CO}_2 + \text{e-} \quad (2)$$

$$\text{Fe}^{3+} + \text{e-} \rightarrow \text{Fe}^{2+} \quad (3)$$

The Mossbauer results however showed that no structural Fe(II) was present in the ferrihydrite + alginate samples (FhA) (see Appendix F).

In summary, gamma irradiation at 5kGy and 28kGy had no influence on the mineralogical characteristics of the Fe-oxides (ferrihydrite, lepidocrocite, and goethite) as confirmed by XRD (Appendix A), Mossbauer analysis (Appendix F), colour (Appendix G) and BET surface area analysis. The amorphous and crystalline structures (Appendix B) were also similar to those reported by Cornell and Schwertmann, 2003 and Frankel *et al*, 2016.

4.2. Addition of the Exopolysaccharide (EPS) Alginate and Percentage of Organic Carbon

At neutral pH, alignate bears a negative charge which caused aggregation of the ferrihydrite, lepidocrocite, and goethite particles (Figure 1-3). Scanning electron microscopy imaging and BET analysis confirmed that there was clumping of the Fe-oxide particles (Appendix B and Table 2). Aggregation of the particles in the presence of alginate led to an increased surface area as shown in Table 2 and impacted the reduction rates (Table 5). All samples containing alginate had faster reduction rates than those without. This is in agreement with the study of Zachara *et al* (2002), Glasauer *et al* (2003), and Shi *et* al (2012), which observed faster Fe (III) reduction rates with the addition of an exopolysaccharide due to increasing the carbon and hydroxyl groups present. The addition of the exopolysaccharide increased the carbon and water content as expected (Table 3), which was validated from the loss of iginition values as indicated by the structural and organic matter values in Table 3. Due to alginate being hydrophilic in complex nanofibers with a rigid chemical structure and sheer viscosity in nature, it acted as an effective polyanionic stabilizer and emulsifier when added to the Fe-oxides, causing coagulation of ferrihydrite, lepidocrocite, and goethite, which increased the latter's ligand-accessible surface area allowing for better binding and structural integrity for bacterial settlements (Appendix B) (Mikutta *et al*, 2008).

4.3. Percent Fraction of Amorphous and Crystalline Fe-Oxides

The series of chemical extractions carried out for the iron speciation of ferrhydrite, lepidocrocite, and goethite yielded amorphous and crystalline fraction results that were different from those determined by Kostka and Luther (1994). According to SEM imaging (Appendix B), the structures of the Fe-oxides are in fact comparable to those in the literature (Schwertmann and Taylor, 1972; Cornell and Schwertmann, 2003), however, once subjected to the chemical extractions (Table 4), it was observed that lepidocrocite and goethite (including the samples containing alginate and gamma

irradiated) had a higher content of amorphous Fe than they should have had, which resulted in higher Fe (III) reduction rates, which contradicts previous studies (Cornell and Schwertmann, 2003). Oxalate and HCl extractions are not reducing agents and therefore were used in combination with hydroxylamine for the determination of amorphous iron, specifically the dissolution of crystalline Fe-oxides in the oxalate extraction if there is Fe (II) in the sample (as a result of an autocatalytic reaction) (Kostka and Luther, 1994). Therefore, these extractions were used as a comparison to the ascorbate and dithionite extractions, which following the protocol of Kostka and Luther (1994) were proven to be more accurate.

Dithionite has the ability to dissolve and reduce, both amorphous and crystalline Fe-oxides and is proven to be effectively used for the determination of the abundance of total iron within the Fe-oxides (mg/gdwt) (ferrihydrite, lepidocrocite, and goethite). The dithionite extraction in conjunction with the ascorbate extraction were used to determine the percent fraction of amorphous and crystalline Fe within all samples of interest. When referring to Table 4, it can be observed that the ascorbate values (amount of amorphous iron (mg/gdwt)) were determined to be “relatively” similar values, which indicates that when applied to the equations to determine the percent fraction of amorphous and crystalline Fe, the final values would be more conducive to a higher percentage of amorphous Fe. With respect to lepidocrocite and goethite, factors affecting the amount of crystalline Fe within the samples include: the over titration of NaOH (lepidocrocite) and the duration in which the Fe-oxide slurry is stirred (goethite) (Cornell and Schwertmann, 2000).

The formation of the Fe-oxides crystal structure is dependent on the synthesis procedure and will affect the percent fraction of amorphous and crystalline Fe proportions determined by the extraction procedures. For example, the chemical extractions are time sensitive prior to determining the speciation of Fe using the ferrozine method, which could have caused the potential for reduction and dissolution to occur causing the extraction techniques to be altered and therefore misrepresent the final

amount of amorphous and crystalline Fe within the Fe-oxide samples. A higher percent fraction of amorphous Fe can be attributed to particle aggregation causing an increase in the reduction rates, which was observed to occur with lepidocrocite (Figure 2) and goethite (Figure 3).

4.4. Anaerobic Reduction of Synthetic BIOS and Synthetic BIOS plus Alginate

Under anaerobic condition, *Shewanella putrefaciens* uses Fe as a terminal electron acceptor to reduce total oxidized Fe (III) species (Roden and Zachara, 1996; Fortin and Langley, 2005; Esther *et al*, 2015). As mentioned above, the rate at which Fe (III) is reduced is influenced by the individual physicochemical properties of the Fe- oxides such as surface area (surface chemistry), crystallinity, and particle size. While it is has been observed in this study that the Fe-oxides underwent no physical or chemical changes when subjected to gamma radiation, there were varied reduction rates observed (Table 5) for the ferrihydrite, lepidocrocite, and goethite samples when compared to past findings (Glasauer *et al*, 2003; Langley *et al*, 2009[A]; Najem *et al*, 2016).

With respect to amount of amorphous Fe, the literature states that an increase in amorphous iron (along with the addition of a EPS) increase the rate of reduction, which can be attributed to an increase in binding sites for *S. putrefaciens* causing direct contact of the bacterial cells and Fe (III) surface and the redox cycling of “electron shuttling” between the bacterial cells and Fe (III) surface (Esther *et al*, 2015). This is important to note because when using *S. putrefaciens*, there is no need for physical contact to occur between *S. putrefaciens* and the Fe (III) surface for reduction to begin and therefore, the more aggregation and amorphous Fe, the easier it is for binding to occur (Langley *et al*, 2009; Esther *et al*, 2015).

The abnormal reduction rates observed for the Fe-oxides, specifically ferrihydrite and goethite, can be attributed to a couple specific factors such as influence from UV-light, “shelf life” of bacteria or genetic drift/transcriptional changes, and subtle variations during the synthesis procedure causing slight

changes to occur to the final Fe-oxide, which can affect the percentage of crystalline and amorphous fractions of each of the Fe-oxide produced. Ultraviolet light (UV) (specifically UVC) on *Shewanella putrefaciens* CN32 has been linked to depletion in bacterial counts, which can cause a variation in the reduction rates of the biotic microcosms causing a light induced reaction (Zachara *et al*, 1998; Qui *et al,* 2004; and Laufer *et al*, 2016). However, the reduction experiments indicate that there was no significant difference ($p > 0.05$) within the reduction rates between non-gamma irradiated ferrihydrite in the presence of UV-light versus those that were in an environment with no direct UV-light (Table 6). There was no visible drop or die off of *Shewanella putrefaciens* CN32 during the reduction experiments, that in concert with the reduction rates calculated would further support the experimental results that UV-light did not negatively impact *Shewanella putrefaciens* CN32 or the reduction rates of the non-gamma irradiated ferrihydrite within this study.

There is a potential for genetic drift, transcriptional variation, and gene expression with the strain of *Shewanella putrefaciens* CN32. To better characterize the strain in the future, the use of rapid amplified polymorphic DNA (RAPD) (used to determine unknown knowledge of DNA sequence) or polymerase chain reaction (PCR) analysis (when DNA sequence is known) can be carried out to confirm that there was no alteration to *Shewanella putrefaciens* CN32 (Ziemke *et al*, 1998). Within the natural environment it is expected to find different strains of *Shewanella* (Brettar and Rheinheimer, 1991). While these variations are expected in nature, they are not likely to occur in the biotic microcosms due to the controlled environment. There is however a possibility that during the inoculation process or the length of storage time the bacteria were kept throughout this study could have caused a genetic change or mutation in the *S. putrefaciens* CN32, thus potentially effecting its fitness and the Fe (III) reduction rates (Roberts *et al*, 2006).

As mentioned earlier, the reduction rates of non- gamma irradiated ferrihydrite varied (Table 5 when compared to past findings. A potential for this variation could be that once the bacteria were added to the biotic microcosms, *S. putrefaciens* CN32 became stressed causing the cells to undergo slower reduction rates for the first week of the reduction experiments, which is then followed by an increase in Fe (III) reduction once *S. putrefaciens* CN32 becomes less stressed and is allowed time to adapt to the environment of the microcosm. This can be observed within Figures 1-3 for all 18 Fe- oxide samples (inclusive of alginate and gamma irradiated samples). After *S. putrefaciens* was allowed to adjust to the microcosm (7-10 days post-inoculation), each microcosm underwent an increase in Fe (III) reduction. The increased time taken by *S. putrefaciens* CN32 to adjust to the goethite and lepidocrocite microcosms along with a potential change to the CN32 strain (such as a possible genetic drift) and the increased percentage of amorphous iron rather than crystalline iron could account for the variation between the reduction rates (Table 6) observed for the goethite and lepidocrocite samples (inclusive of alginate and gamma-irradiated samples) during the biotic microcosm experiments when compared to those from the literature (Zachara *et al*, 2002; Glasauer *et al*, 2003).

Dichristina (1992) indicated that there could be inhibitory effects when using *S. putrefaciens* in a medium containing nitrogen which can slow the Fe^{3+} reduction under laboratory anaerobic conditions. As mentioned above, the decreased reaction rates 7-10 days post inoculation could be attributed to the findings of Dichristina (1992) because in the chemically defined medium (CDM), the stock solution 1 contained ammonium chloride (NH_4Cl_2), which could have potentially complexed with the other trace elements in the stock solution 2. While this could explain the decreased Fe^{3+} reduction rates for Fh and FhA, ion chromatography analyses confirmed that there were no important amounts of nitrogen compounds (Appendix H) within the medium that could have led *S. putrefaciens* CN32 to preferentially reduce NO_3^- over Fe^{3+}.

The determined amount of amorphous iron in goethite and lepidocrocite suggests that the synthesis procedure may have led to the formation of poorly ordered iron oxides such as ferrihydrite. However, when analyzing the X-ray diffraction patterns for all goethite and lepidocrocite samples, it was concluded that all samples were in fact the minerals goethite and lepidocrocite (Schwertmann and Cornell, 2003). However, the 2 main diffraction peaks of ferrihydrite are close to those of goethite and ferrihydrite, it is therefore possible that ferrihydrite was present within the more crystalline samples, but it could not be identified by XRD. Fe-EXAFS analyses would have been needed to quantify the amount of ferrihydrite in the samples. According to Glasauer *et al*. (2003), it was observed that under anaerobic conditions, *S. putrefaciens* CN32 reduced hydrous ferric oxides but they observed no Fe (III) reduction of poorly ordered nanometer and well-ordered micron-sized goethite over a 46 day period. While XRD confirmed the crystallography of poorly crystalline G and GA (Cornell and Schwertmann, 2000), there was likely variability within the experimental process, such as the ageing of the Fe-oxides between the synthesis and the biotic experiment, the potential transformation of goethite to hematite, and the potential of more poorly sorted amorphous iron present in the synthesized nano- and micro-goethite by (Glasauer *et al*, 2003).

While the chemical extraction procedures are clearly laid out by Kostka and Luther (1994) (Appendix D) for the ascorbate and dithionite extractions (used to estimate the amount of amorphous and crystalline Fe-oxides), there may have been variations during the overall execution of the extraction procedures, thus affecting the end results of the chemical extraction and the estimation of the final percentage of amorphous and crystalline Fe. Variations during the chemical extraction procedures that could have caused discrepancies include: ill preparation of extraction solutions, ascorbate and oxalate samples effected by UV-light, the duration of the sample incubation during the ferrozine assay speciation, and the improper execution of the extraction protocols. These, in conjunction with the potential genetic drift or transcriptional variation of *S. putrefaciens* CN32, possibly explain the lower

reduction rates observed for ferrihydrite when compared to those of Langley *et al* (2009[C]) and the increased reduction rates of the more crystalline goethite due to the potential presence of amorphous Fe in the form of ferrihydrite (Table 4).

In summary, several experimental errors might have occurred during the biotic reduction of the various iron oxides. These include a lack of full extraction during the strong HCl chemical extraction to determine the amount of Fe-oxide needed for the reduction experiments (in order to maintain a concentration of 4mM within the microcosm), change in the chemically defined medium (CDM) overtime (potential precipitation), presence of oxygen during the anaerobic reduction, error in the spectrophotometer analysis causing inadequate absorbance values thus causing an incorrect amount of *S. putrefaciens* CN32 cells and Fe-oxide to be added to the microcosms, genetic/ transcriptional variations of *S. putrefaciens* CN32 used for this study, and error within the synthesis procedures. Therefore, while an effective dosage level of gamma irradiation was achieved, there needs to be more research carried out to better understand the microbial interaction of *S. putrefaciens* CN32 with the more crystalline Fe-oxides of goethite and lepidocrocite.

4.5. Current and Future Work

4.5.1. Research Areas that Require Microbial Sterilization

Effective sterilization of microorganisms is a vital procedure for a wide array of applications within many different research fields. For example, within the agricultural industry, from a production/food safety perspective, gamma ray sterilization is used to remove soil and air borne microorganisms that may be unsafe for ingestion because its ionizing energy allows for rapid and efficient penetration through polysaccharides and microbial life (Piri *et al*, 2011). Within the agricultural industry, the effective dosage limit is approximately 5-15kGy in order to remove microorganisms without adversely affecting post-harvest yields via functional and structural changes, which is also within

the gamma irradiation threshold for this study (Bank *et al*, 2008; Piri *et al*, 2011). This suggests that the gamma irradiation threshold used within the agricultural industry can be expanded to 28kGy as there were no structural or physicochemical changes to the Fe-oxides observed within this study. However, it must be noted that these levels are only valid for post-harvested yield ready for distribution because plants exposed to gamma irradiation prior to harvest will have altered seed germination, growth, and development (Marcu *et* al, 2013). It is recommended to subject those seeds to gamma irradiation levels of ≤0.5 kGy (Marcu *et* al, 2013).

Gamma irradiation is extensively used within the medical and pharmaceutical industry for the sterilization of surgical equipment, plastics, wasteform materials, and consumables (McGann *et* al, 2012; Sandle and Saghee, 2012; Brown *et al*, 2014). The purpose is to decontaminate the products and waste by breaking down DNA at the molecular level and reducing bacterial mutation. Again, determining a dosage threshold (specifically a maximum dosage) is needed to ensure that there is no degradation to the packaging of surgical equipment and to reduce the amount of free radicals produced during waste storage, plastics sterilization, and disposal to effectivity maintain the integrity of the products and reduce harmful by-products from storage and disposal, which can be chemically leached into the environment (McGann *et* al, 2012; Sandle and Saghee, 2012). For wasteform materials, McGann *et* al, 2012 observed that at a high dosage (8MGy) of gamma irradiation, there was no mechanical stability or compositional concern. However, Brown *et al*, 2014 observed that at the nanoscale level of ferrihydrite, lepidocrocite, and goethite, Fe-oxide samples subjected to gamma irradiation beyond 1MGy will undergo transformation, thus affecting the physicochemical properties of the Fe-oxides.

4.5.2. Future Research into Microbial Reduction, Bioremediation, and Biomining

In the last few years, microbial processes involving the interactions between microorganisms and Fe-oxides (specifically BIOS), transitional metals and metalloids have been heavily studied because they can be used in bioremediation and metal extraction strategies in the mining and processing sectors

(Lee *et al*, 2012; Navarro *et al*, 2013; Sanchez-Andrea *et al*, 2016). In addition, the increase in industrialization has led to negative environmental impacts and increased metal contamination to various areas such as: oil storage facilities, mining sites, waste disposal repositories, soils, water, and sediments etc. (Lee *et al*, 2012). From a bioremediation perspective, anaerobic conditions (e.g. saturated soil/ sediments and bioreactors) can lead to the reduction of Fe-oxides (known to sorb metal contaminants) due to the fact that they are a terminal electron acceptor for several metal reducing bacteria (e.g. *Shewanella putrefaciens* CN32, *Geobacter metallireducens,* etc.). Sorbed metals (e.g. Co, Mn, Ni, Zn, As(III), As(V), Cr(III), U(VI), Cr(VI) etc.) released during the reduction can later precipitate or be immobilized by secondary minerals formed during the reduction within biofilms, which has been observed in natural subsurface environments (e.g. acid mine drainage) (Lee *et al*, 2012; Navarro *et al*, 2013; Johnson *et al*, 2013).

The overburden containing toxic metals and waste produced by the mining industry are an important environmental issue. Bioremediation using microorganisms could be used to aid in the rehabilitation during the life cycle of a mining project. If applied at an industrial scale to precipitate metals from the mineral extraction process, tailings ponds, acid mine drainage, and other mineral leachates, it could lead to an improvement in metal recovery. Consequently, this process could enhance the efficiency of the primary ore extraction process and reduce the overall mineral waste produced and environmental contamination (Sanchez-Andrea *et al*, 2016). Biomining is a general term used to describe the use of microorganisms used to facilitate the extraction of iron-containing ores or concentrate (Johnson *et al*, 2013; Sanchez-Andrea *et al*, 2016).

The results from this study further aid our understanding of the reductive and physicochemical properties of 2-line ferrihydrite, lepidocrocite, and goethite, which can be used in the future for bioremediation and biomining research. Better understanding of the reduction of ferric iron within anaerobic environments may prove to be useful due to the over saturation of soils, sediments, tailings

ponds, and acid mine drainage with metals and metalloids causing the surrounding environment to potentially be slightly more acidic and depleted in oxygen. Further research needs to be undertaken to better understand microbial reduction of more crystalline Fe-oxides such as goethite and lepidocrocite. This could aid in the understanding of what metals are most likely to be incorporated into the lattice structure of the Fe-oxides (specifically goethite) by adsorption, co-adsorption, adhesion, and co-precipitation, all of which can affect the retention, bioavailability, and bioaccumulation of oxyanions in the natural environments (Johnson *et al*, 2013; Mikutta *et al*, 2014). Within naturally occurring ferrihydrite, along with inorganic impurities, there is natural organic matter present which can affect the affinity, crystallinity, particle size, solubility and aggregation properties of natural iron oxides (Mikutta *et al*, 2014).

This study used the EPS alginate during the synthesis of iron oxides in order to mimic the organic matter present in natural biogenic iron oxides. However, more research is needed into this EPS along with others to better understand, specifically from a bioremediation and biomining perspective, how exopolysaccharides within the anaerobic environment and in conjunction with microorganisms effect the electron shuttling to Fe (III) and the solubilizing of iron causing a variation in the reduction of Fe (III) and metals that will be incorporated into the lattice structure and precipitated out as a biofilm (Luu *et al*, 2003; Lee *et al*, 2012).

4.6. Conclusions

The ability to provide an efficient sterilization dosage threshold for gamma irradiation is crucial to ensure that there is no degradation or physicochemical alterations to the sample of interest that can negatively affect the experimental results. The results of this study concluded that a dosage of 5 and 28kGy were sufficient dosage levels for the removal of microbial activity without adversely affecting the Fe-oxides ferrihydrite, lepidocrocite, and goethite. Studies conducted on bacteriogenic iron oxides (BIOS), food production, and medical tools have provided detailed insight into similar sterilization

techniques however, this study further validates in concert with previous literature, that gamma irradiation is an efficient mode of sterilization for natural Fe-oxides (amorphous and crystalline).

Chemical extractions performed on the synthetic BIOS samples revealed that there was a higher amorphous Fe content, which is expected for 2-line ferrihydrite due to its poorly ordered amorphous structure. However, the amorphous Fe percentage was determined to be very high for the supposedly more crystalline Fe-oxides lepidocrocite and goethite. The increased amorphous Fe content increased the bioavailable Fe, aggregation, and surface area thus making lepidocrocite and goethite more susceptible to microbial reduction. The percent Fe fraction determined by the chemical extraction procedures is open to scrutiny, not necessarily the protocol itself, but the execution of the extraction protocols outline in section 4.3, as human error can never be fully negated. It is also possible that small amounts of ferrihydrite formed during the synthesis of goethite and lepidocrocite, which would explain their higher than expected amorphous content and their higher reductions rates than those in the literature.

Finally, it was observed that the addition of alginate during the synthesis of the various iron oxides led to an overall increase in Fe (III) reduction rates for all Fe-oxides when compared to the non-alginate samples. Surface area measurements indicated that alginate caused the surface area to increase, which in turn can enhance the rates of reduction as observed in other studies.

References

Bank, T. L.; Kukkadapu, R. K.; Madden, A. S.; Ginder-Vogel, M. A.; Baldwin, M. E.; Jardine, P. M. Effects of gamma-sterilization on the physicochemical properties of natural sediments. *Chem. Geol.* **2008**, *251* (1–4), 1–7.

Berg, J.M.; Tymoczko, J. L; Stryer, L. Biochemistry. 5th Edition. *New York, New York: W.H. Freeman and Company*. **2002**.

Brettar, I.; Rheinheimer, G. Denitrification in the central Baltic: evidence for H2 S-oxidation as motor of denitrification at the oxic-anoxic interface. *Mar. Ecol. Prog. Ser.* **1991**, *77* (2–3), 157–169.

Brown, A. R.; Wincott, P. L.; Laverne, J. A.; Small, J. S.; Vaughan, D. J.; Pimblott, S. M.; Lloyd, J. R. The impact of gamma radiation on the bioavailability of Fe (III) minerals for microbial respiration. *Environ. Sci. Technol.* **2014**, *48* (18), 10672–10680.

Buchan, D.; Moeskops, B.; Ameloot, N.; De Neve, S.; Sleutel, S. Selective sterilisation of undisturbed soil cores by gamma irradiation: Effects on free-living nematodes, microbial community and nitrogen dynamics. *Soil Biol. Biochem.* **2012**, *47*, 10–13.

Chambers, D. P.; Attiwill, P. M. The ash-bed effect in Eucalyptus regnans forest: Chemical, physical and microbiological changes in soil after heating or partial sterilisation. *Aust. J. Bot.* **1994**, *42* (6), 739–749.

Châtellier, X.; West, M. M.; Rose, J.; Fortin, D.; Leppard, G. G.; Ferris, F. G. Characterization of Iron-Oxides Formed by Oxidation of Ferrous Ions in the Presence of Various Bacterial Species and Inorganic Ligands. *Geomicrobiol. J.* **2004**, *21* (2), 99–112.

Cismasu, A. C.; Levard, C.; Michel, F. M.; Brown, G. E. Properties of impurity-bearing ferrihydrite II: Insights into the surface structure and composition of pure, Al- and Si-bearing ferrihydrite from Zn(II) sorption experiments and Zn K-edge X-ray absorption spectroscopy. *Geochim. Cosmochim. Acta.* **2013**, *119*, 46–60.

Cornell, R. M.; Schwertmann, U. Iron Oxides in the Laboratory: Preparation and Characterization. 2nd Edition. *Wienheim, Germany: Wiley*-VCH. **2000**.

Cornell, R. M.; Schwertmann, U. The Iron Oxides: Structure, Properties, Reaction, Occurrence and Uses. 2nd Edition. *Wienheim, Germany: Wiley*-VCH. **2003**.

DiChristina, T. J. Effects of nitrate and nitrite on dissimilatory iron reduction by Shewanella putrefaciens 200. *J. Bacteriol.* **1992**, *174* (6), 1891–1896.

Dzaugis, M. E.; Spivack, A. J.; D'Hondt, S. A quantitative model of water radiolysis and chemical production rates near radionuclide-containing solids. *Radiat. Phys. Chem.* **2015**, *115*, 127–134.

Esther, J.; Sukla, L. B.; Pradhan, N.; Panda, S. Fe (III) reduction strategies of dissimilatory iron reducing bacteria. *Korean J. Chem. Eng.* **2014**, *32* (1), 1–14.

Frankel, R. B; Faivre, D. Iron Oxides: From Nature to Applications. *Wienheim, Germany: Wiley*-VCH. **2016**.

Ferris, F. G. Biogeochemical Properties of Bacteriogenic Iron Oxides. *Geomicrobiol. J.* **2005**, *22* (3–4), 79–85.

Fortin, D.; Langley, S. Formation and occurrence of biogenic iron-rich minerals. *Earth-Science Rev.* **2005**, *72* (1–2), 1–19.

Gault, A. G.; Ibrahim, A.; Langley, S.; Renaud, R.; Takahashi, Y.; Boothman, C.; Lloyd, J. R.; Clark, I. D.; Ferris, F. G.; Fortin, D. Microbial and geochemical features suggest iron redox cycling within bacteriogenic iron oxide-rich sediments. *Chem. Geol.* **2011**, *281* (1–2), 41–51.

Glasauer, S.; Langley, S.; Beveridge, T. J. Sorption of Fe (Hydr) Oxides to the Surface of Shewanella putrefaciens : Cell-Bound Fine-Grained Minerals Are Not Always Formed De Novo Sorption of Fe (Hydr) Oxides to the Surface of Shewanella putrefaciens : Cell-Bound Fine-Grained Minerals Are Not A. *Appl. Environ. Microbiol.* **2001**, *67* (12), 5544–5550.

Glasauer, S.; Weidler, P. G.; Langley, S.; Beveridge, T. J. Controls on Fe reduction and mineral formation by a subsurface bacterium. *Geochim. Cosmochim. Acta*. **2003**, *67* (7), 1277–1288.

Gournis, D.; Mantaka-Marketou, a E.; Karakassides, M. a; Petridis, D. Effect of γ-irradiation on clays and organoclays: a Mössbauer and XRD study. *Phys. Chem. Miner.* **2000**, *27*, 514-521.

Johnson, D.; Grail, B.; Hallberg, K. A New Direction for Biomining: Extraction of Metals by Reductive Dissolution of Oxidized Ores. *Minerals*. **2013**, *3* (1), 49–58.

Kasama, T.; Murakami, T. The effect of microorganisms on Fe precipitation rates at neutral pH. *Chem. Geol.* **2001**, *180* (1–4), 117–128.

Kennedy, C. B.; Gault, A. G.; Fortin, D.; Clark, I. D.; Ferris, F. G. Retention of Iodide by Bacteriogenic Iron Oxides. *Geomicrobiol. J.* **2011**, *28* (5–6), 387–395.

Klassen, N. V; Shortt, K. R.; Seuntjens, J.; Ross, C. K. Fricke dosimetry: the difference between $G(Fe^{3+})$ for ^{60}Co gamma-rays and high-energy x-rays. *Phys. Med. Biol.* **1999**, *44* (7), 1609–1624.

Komlos, J.; Kukkadapu, R. K.; Zachara, J. M.; Jaffé, P. R. Biostimulation of iron reduction and subsequent oxidation of sediment containing Fe-silicates and Fe-oxides: Effect of redox cycling on Fe (III) bioreduction. *Water Res.* **2007**, *41* (13), 2996–3004.

Kostka, J.E.; Luther, G.W. Partitioning and speciation of solid phase iron in saltmarsh sediments. *Geochim. Cosmochim. Acta.* **1994**, *58* (7), 1701–1710.

Lamm, C. G. Applications of Isotopes and Radiation in Agriculture . *Iaea Bull.* **2007**, *2* (2), 29–35.

Langley, S.; Igric, P.; Takahashi, Y.; Sakai, Y.; Fortin, D.; Hannington, M. D.; Schwarz-Schampera, U. Preliminary characterization and biological reduction of putative biogenic iron oxides (BIOS) from the Tonga-Kermadec Arc, southwest Pacific Ocean. *Geobiology* **2009**[A], *7* (1), 35–49.

Langley, S.; Gault, A. G.; Ibrahim, A.; Takahashi, Y.; Renaud, R.; Fortin, D.; Clark, I. D.; Ferris, F. G. Strontium desorption from bacteriogenic iron oxides (BIOS) subjected to microbial Fe(III) reduction. *Chem. Geol.* **2009**[B], *262* (3–4), 217–228.

Langley, S.; Gault, A.; Ibrahim, A.; Renaud, R.; Fortin, D.; Clark, I. D.; Ferris, F. G. A Comparison of the Rates of Fe (III) Reduction in Synthetic and Bacteriogenic Iron Oxides by *Shewanella putrefaciens* CN32. *Geomicrobiol. J.* **2009**[C], *26* (2), 57–70.

Laufer, K.; Roy, H.; Jorgensen, B. B.; Kappler, A. Evidence for the existence of autotrophic nitrate-reducing Fe(II)-oxidizing bacteria in marine coastal sediment. *Appl. Environ. Microbiol.* **2016**, *82* (20), 6120–6131.

Le Caër, S. Water Radiolysis: Influence of Oxide Surfaces on H2 Production under Ionizing Radiation. *Water* **2011**, *3* (4), 235–253.

Luu, Y.; Ramsay, B. A.; Ramsay, J. A. Nitrilotriacetate stimulation of anaerobic Fe(III) respiration by mobilization of humic materials in soil. *Appl. Environ. Microbiol.* **2003**, *69* (9), 5255–5262.

Marcu, D.; Damian, G.; Cosma, C.; Cristea, V. Gamma radiation effects on seed germination, growth and pigment content, and ESR study of induced free radicals in maize (Zea mays). *J. Biol. Phys.* **2013**, *39* (4), 625–634.

McGann, O. J.; Bingham, P. A.; Hand, R. J.; Gandy, A. S.; Kavcic, M.; Zitnik, M.; Bucar, K.; Edge, R.; Hyatt, N. C. The effects of gamma-radiation on model vitreous waste-forms intended for the disposal of intermediate and high level radioactive wastes in the United Kingdom. *J. Nucl. Mater.* **2012**, *429* (1–3), 353–367.

McNamara, N. P.; Black, H. I. J.; Beresford, N. A.; Parekh, N. R. Effects of acute gamma irradiation on chemical, physical and biological properties of soils. *Appl. Soil Ecol.* **2003**, *24* (2), 117–132.

Mikutta, C.; Mikutta, R.; Bonneville, S.; Wagner, F.; Voegelin, A.; Christl, I.; Kretzschmar, R. Synthetic coprecipitates of exopolysaccharides and ferrihydrite. Part I: Characterization. *Geochim. Cosmochim. Acta*. **2008**, *72* (4), 1111–1127.

Mikutta, R.; Lorenz, D.; Guggenberger, G.; Haumaier, L.; Freund, A. Properties and reactivity of Fe-organic matter associations formed by co-precipitation versus adsorption: Clues from arsenate batch adsorption. *Geochim. Cosmochim. Acta.* **2014**, *144*, 258–276.

Najem, T.; Langley, S.; Fortin, D. A comparison of Fe(III) reduction rates between fresh and aged biogenic iron oxides (BIOS) by Shewanella putrefaciens CN32. *Chem. Geol.* **2016**, *439*, 1–12.

Navarro, C. A.; von Bernath, D.; Jerez, C. A. Heavy metal resistance strategies of acidophilic bacteria and their acquisition: Importance for biomining and bioremediation. *Biol. Res.* **2013**, *46* (4), 363–371.

O'Connor, D. A. The Mossbauer Effect. *Contemp. Phys.* **1968**, *9* (6), 521–535.

Plotze, M.; Kahr, G.; Hermanns Stengele, R. Alteration of clay minerals - gamma-irradiation effects on physicochemical properties. *Appl. Clay Sci.* **2003**, *23* (1–4), 195–202.

Qiu, X.; Sundin, G. W.; Chai, B.; Tiedje, J. M. Survival of Shewanella oneidensis MR-1 after UV Radiation Exposure. **2004**, *70* (11), 6435–6443.

Ramsay, A. J.; Bawden, A. D. Effects of sterilization and storage on respiration, nitrogen status and direct counts of soil bacteria using acridine orange. *Soil Biol. Biochem*. **1983**, 15 (3), 263–268.

Lee, B.; Baltrusaitis; Ray J. R J.; Jun, Y. S. Formation of iron(III) (hydr)oxides on polyaspartate- and alginate-coated substrates: Effects of coating hydrophilicity and functional group. *Environ. Sci. Technol.* **2012**, *46* (24), 13167–13175.

Roberts, J. A.; Fowle, D. A.; Hughes, B. T.; Kulczycki, E. Attachment Behavior of *Shewanella putrefaciens* onto Magnetite under Aerobic and Anaerobic Conditions. *Geomicrobiol. J.* **2006**, *23* (8), 631–640.

Roden, E. E.; Zachara, J. M. Microbial reduction of crystalline iron (III) oxides: Influence of oxide surface area and potential for cell growth. *Env. Sci Technol*. **1996**, *30* (5), 1618–1628.

Sanchez, I. S.; Stams, A. J.; Weijma, J.; Contreras, P. G.; Dijkman, H.; Rozendal, R. A.; Johnson, D. B. *FEMS. Micro*. **2016**, *363*, 1–4.

Sandle, T.; Saghee, M.R. Application of Sterilization of Gamma Radiation for Single-Use Disposable Technologies in the Biopharmaceutical Sector. *GXP. Compliance*. **2012**, *16* (2), 60–68.

Schaller, J.; Weiske, A.; Dudel, E. G. Effects of gamma-sterilization on DOC, uranium and arsenic remobilization from organic and microbial rich stream sediments. *Sci. Total Environ.* **2011**, *409* (17), 3211–3214.

Schwertmann, U.; Taylor, R. M. The transformation of lepidocrocite to goethite. *Clays Clay Miner.* **1972**, *20* (3), 151–158.

Shi, L.; Rosso, K. M.; Clarke, T. A.; Richardson, D. J.; Zachara, J. M.; Fredrickson, J. K. Molecular underpinnings of Fe(III) oxide reduction by Shewanella oneidensis MR-1. *Front. Microbiol.* **2012**, *3* (2), 1–10.

Stookey, L. L. Ferrozine: a new spectrophotometric reagent for iron. *Anal. Chem.* **1970**, *42* (7), 779–781.

Vandegrift, G.; Fultz, B. The Mossbauer Effect Explained. *Am. J. Phys.* **1998**, *66* (7), 593–596.

Zänker, H.; Richter, W.; Huttig, G. Scavenging and immobilization of trace contaminants by colloids in the waters of abandoned ore mines. *Colloids Surfaces A Physicochem. Eng. Asp.* **2003**, *217* (1–3), 21–31.

Zachara, J. M.; Fredrickson, J. K.; Li, S. M.; Kennedy, D. W.; Smith, S. C.; Gassman, P. L. Bacterial reduction of crystalline Fe^{3+} oxides in single phase suspensions and subsurface materials. *Am. Mineral.* **1998**, *83* (11–12 PART 2), 1426–1443.

Zachara, J. M.; Kukkadapu, R. K.; Fredrickson, J. K.; Gorby, Y. A.; Smith, S. C. Biomineralization of Poorly Crystalline Fe(III) Oxides by Dissimilatory Metal Reducing Bacteria (DMRB). *Geomicrobiol. J.* **2002**, *19* (2), 179–207.

Ziemke, F.; Hofle, M. G.; Lalucat, J.; Rossello-moras, R. Reclassification of *Shewanella putrefaciens* Owen's genomic group II as *Shewanella baltica* sp.nov. *Internat. J. Syst. Bacteriol.* **1998**, *48* (1 998), 179–186.

Appendix A: X-Ray Diffractograms of Ferrihydrite, Lepidocrocite, and poorly crystalline Goethite (Pre/Post Reductions).

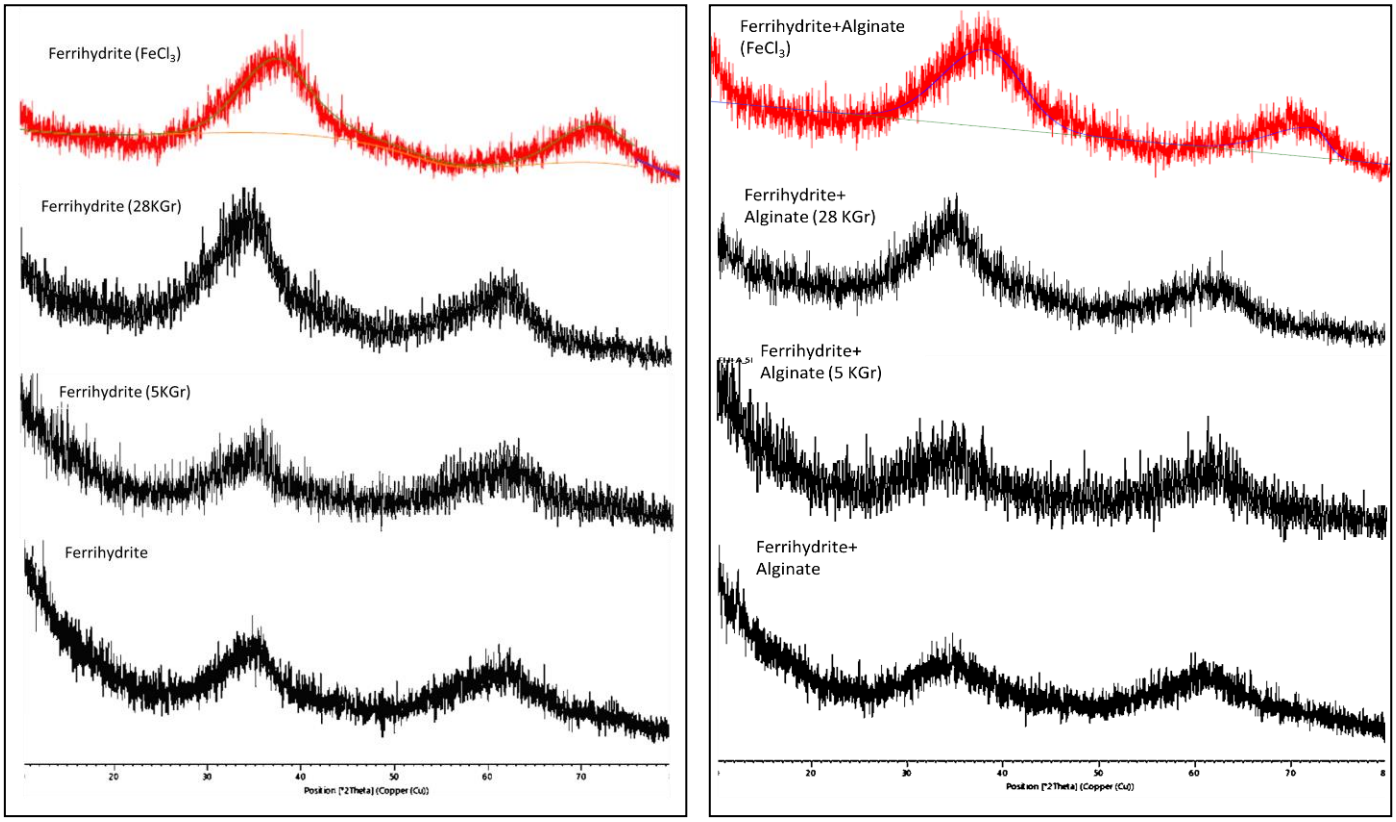

Figure A-1: X-Ray Diffractograms of 2-line Ferrihydrite with and without the addition of Alginate.

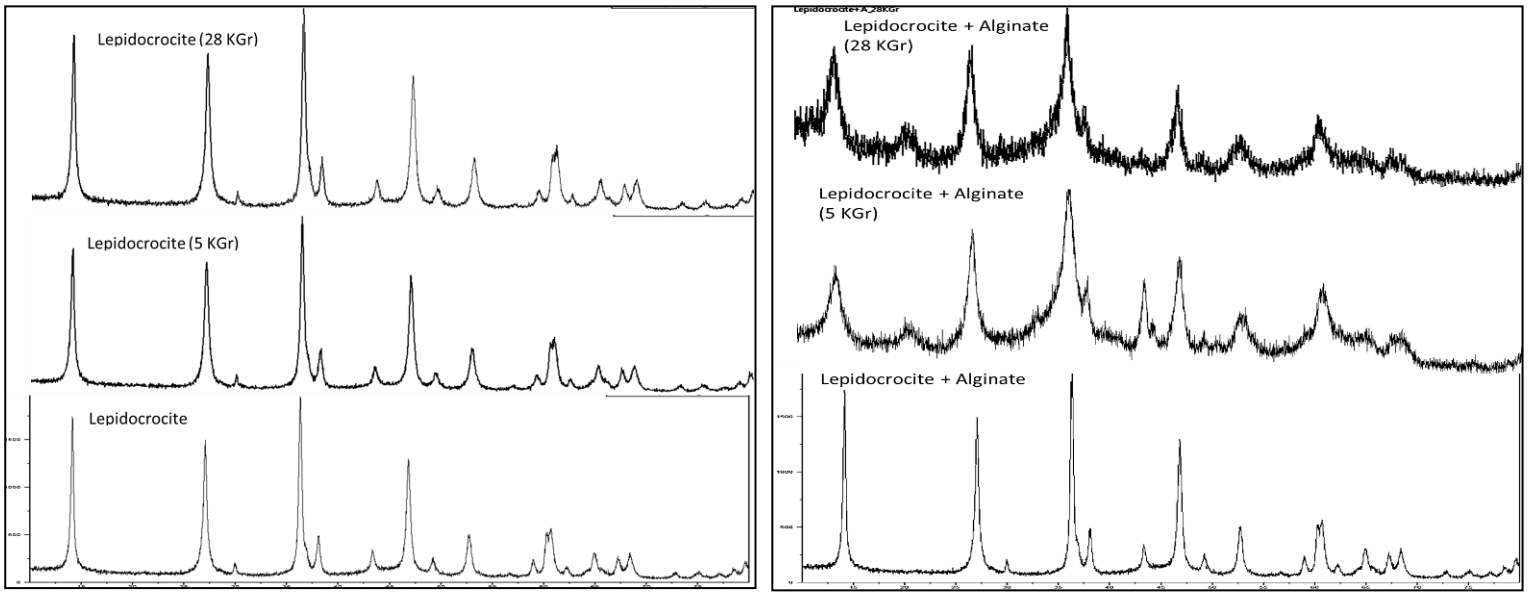

Figure A-2: X-Ray Diffractograms of Lepidocrocite with and without the addition of Alginate.

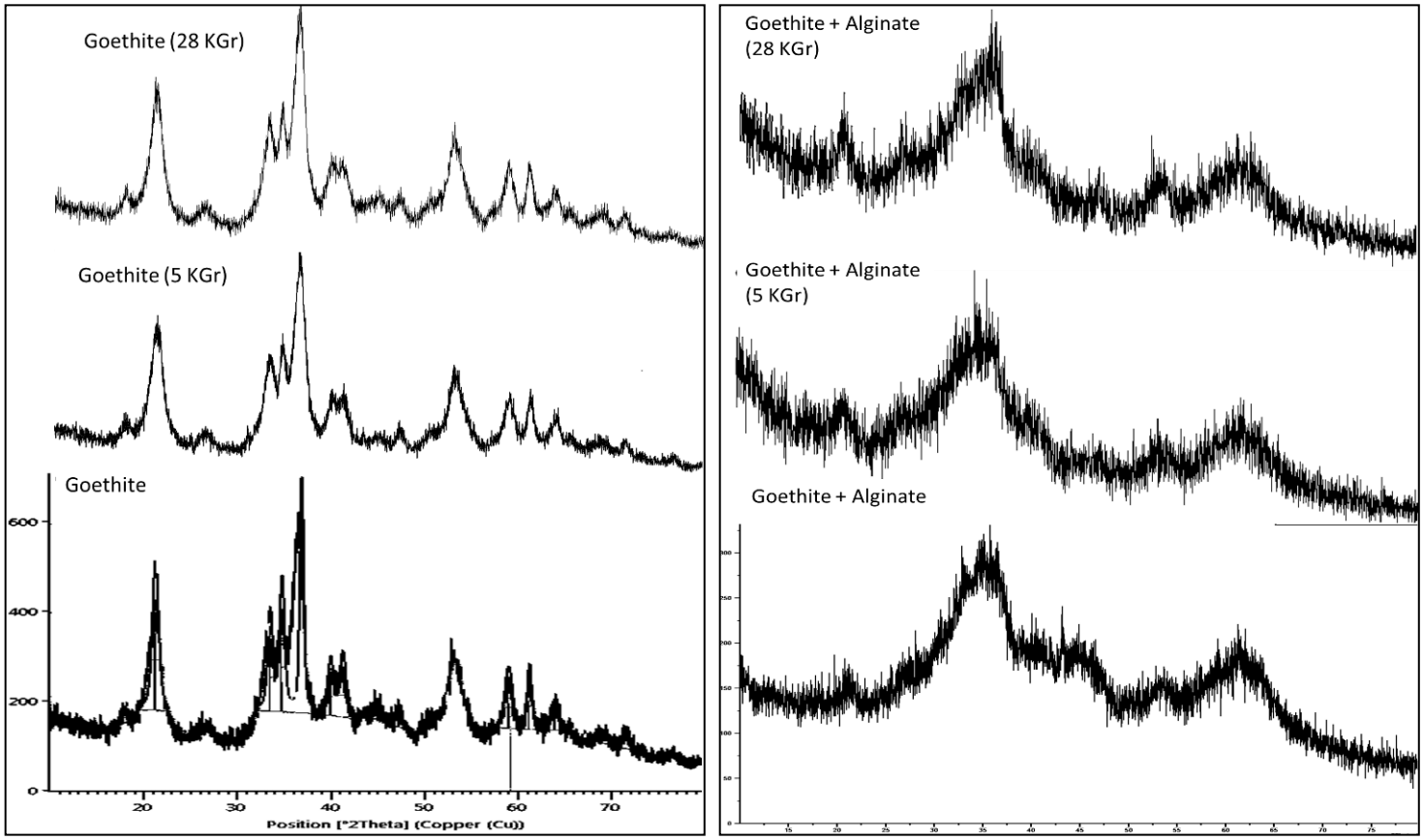

Figure A-3: X-Ray Diffractograms of Goethite with and without the addition of Alginate.

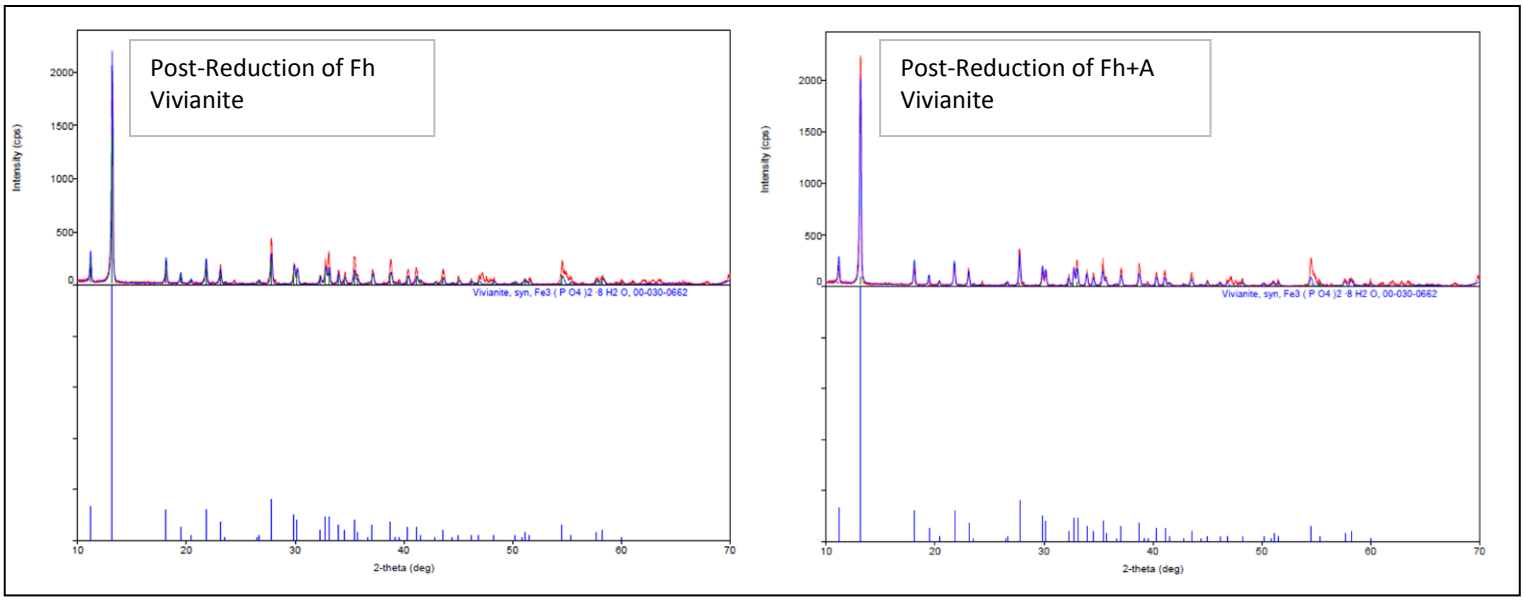

Figure A-4: X-Ray Diffractograms of 2-line Ferrihydrite with and without the addition of Alginate post microbial reduction to produce Vivianite.

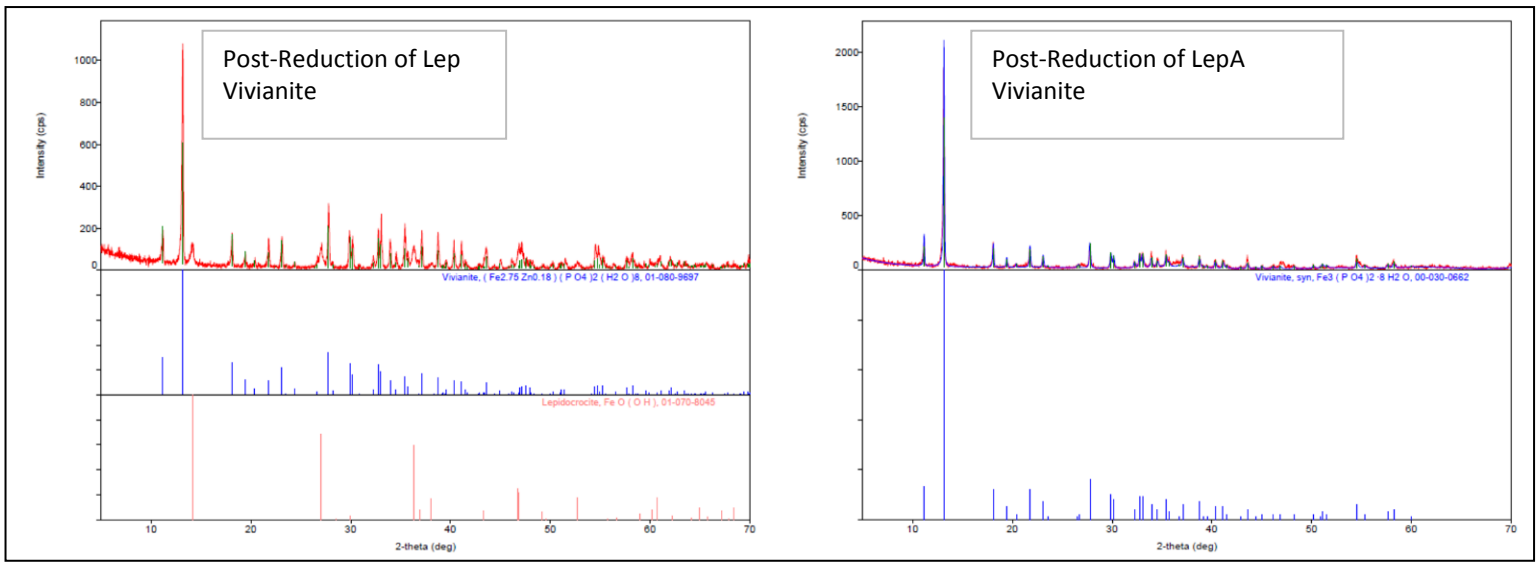

Figure A-5: X-Ray Diffractograms of Lepidocrocite with and without the addition of Alginate post microbial reduction to produce Vivianite.

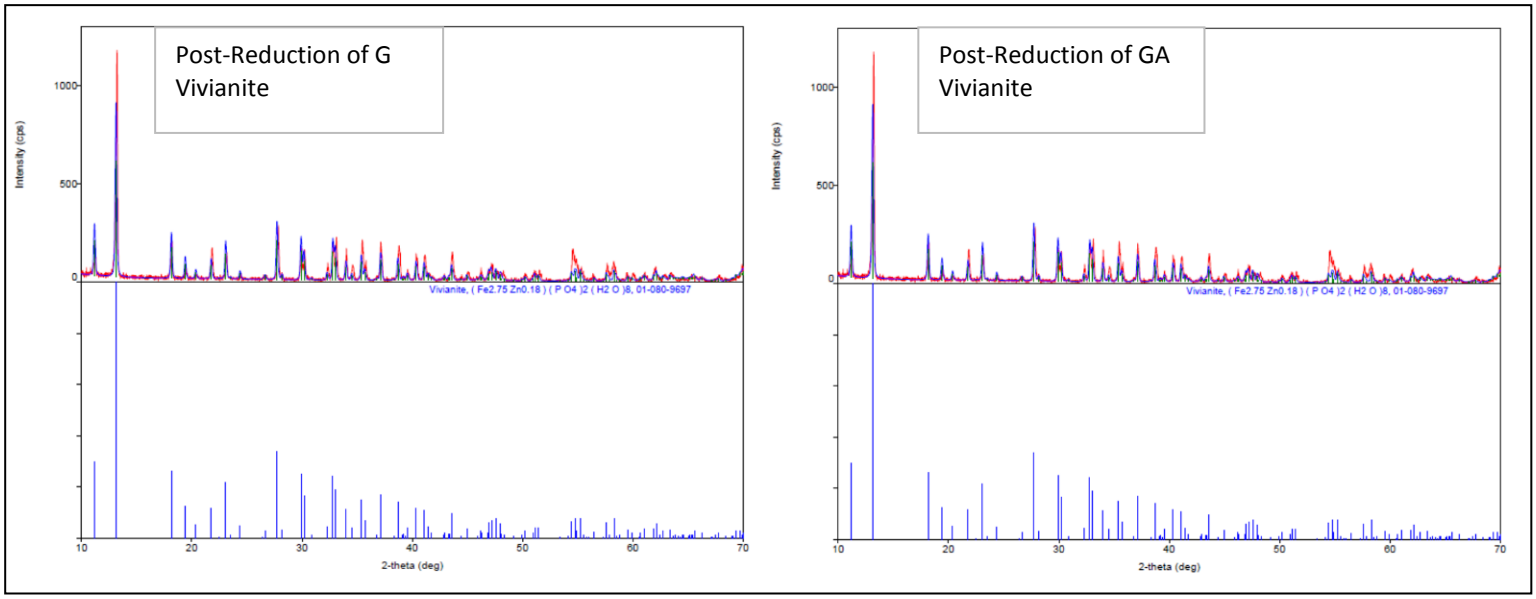

Figure A-6: X-Ray Diffractograms of Goethite with and without the addition of Alginate post microbial reduction to produce Vivianite.

Appendix B: Scanning Electron Microscope (SEM) images of Ferrihydrite, Lepidocrocite, and Goethite with and without the presence of the EPS Alginate.

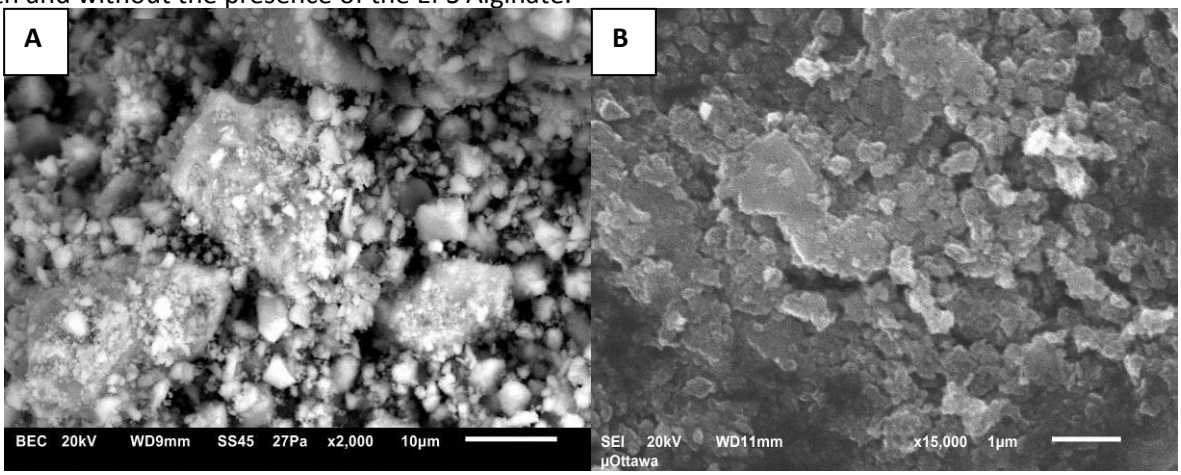

Figure B-1: Scanning Electron Microscopy (SEM) images of Ferrihydrite (Left: Fh, Right: FhA).

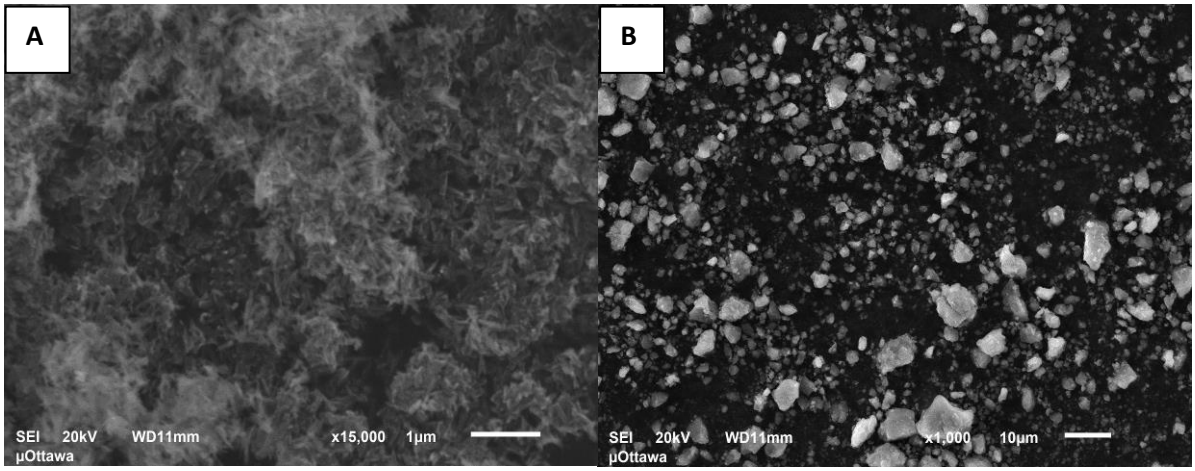

Figure B-2: Scanning Electron Microscopy (SEM) images of Lepidocrocite (Left: Lep, Right: LepA).

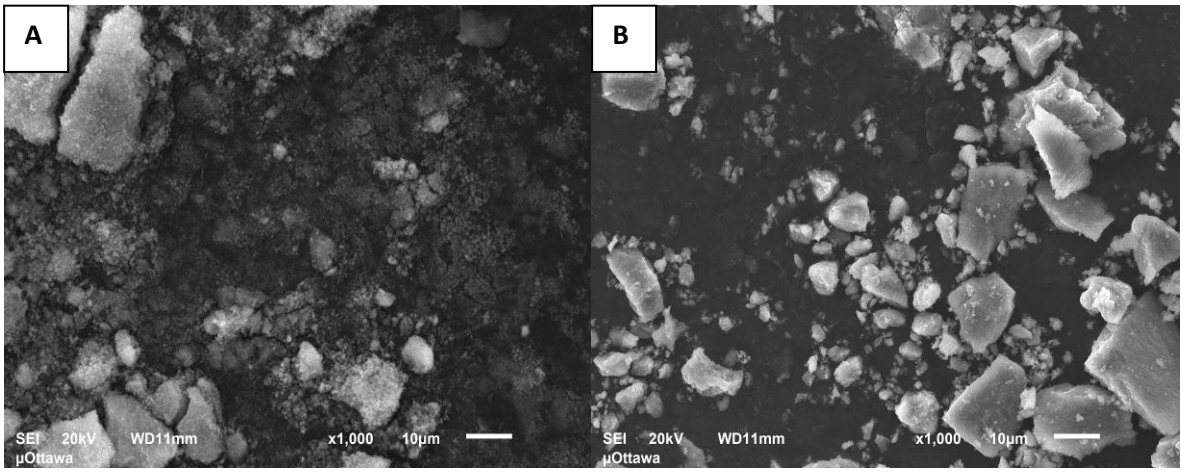

Figure B-3: Scanning Electron Microscopy (SEM) images of Goethite (Left: G, Right: GA).

Appendix C: Quality Control Reduction experiments to test the use of a Ferric Nitrate salt for synthesis and the effect of Sunlight along with and Aged vs. Fresh inoculum of *S. putrefaciens* CN32.

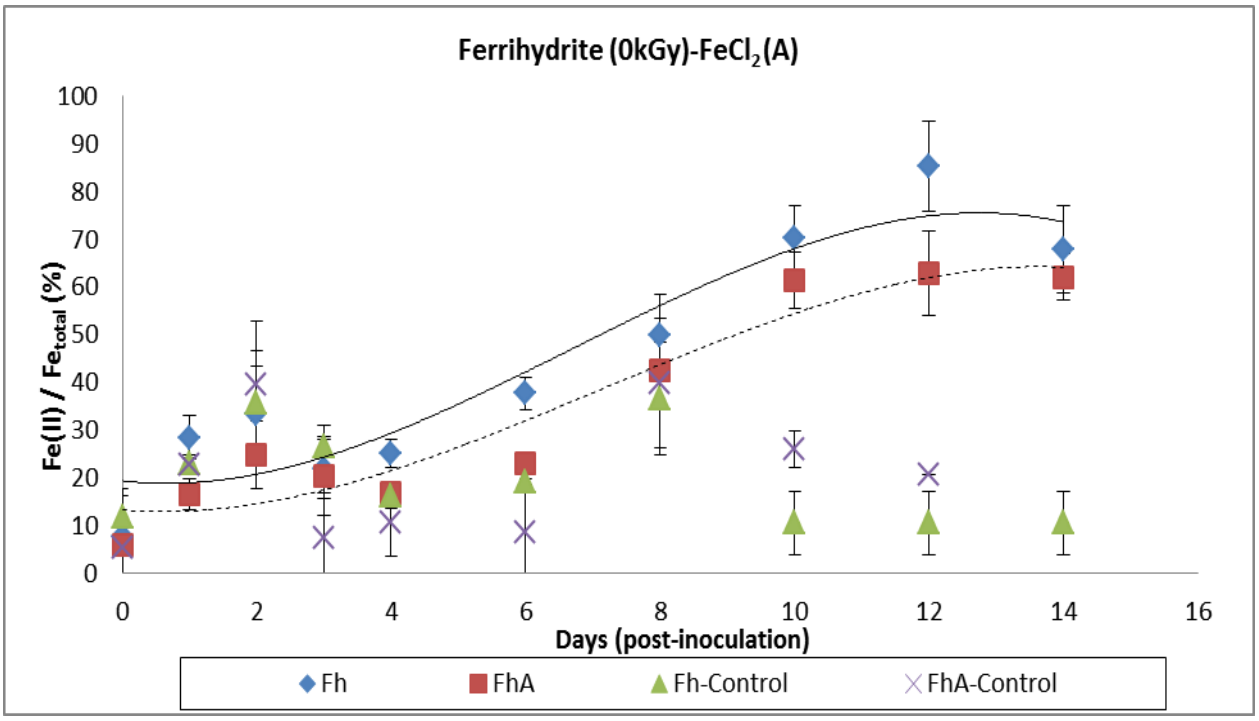

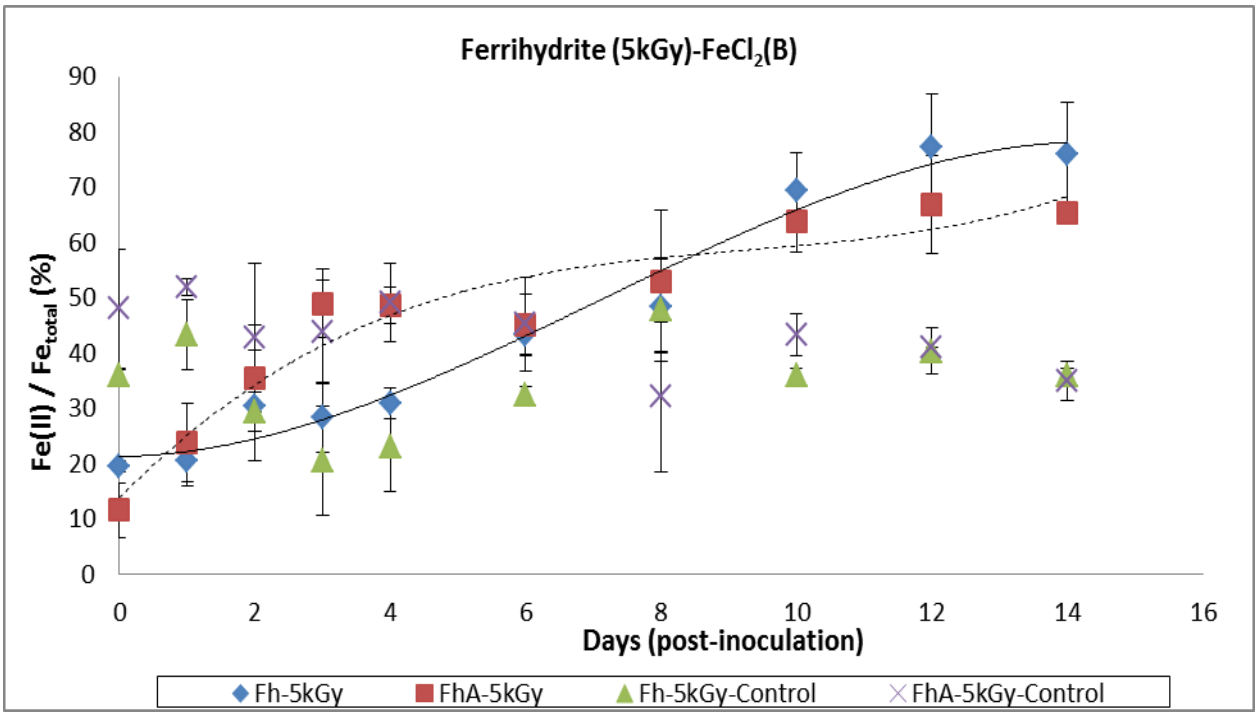

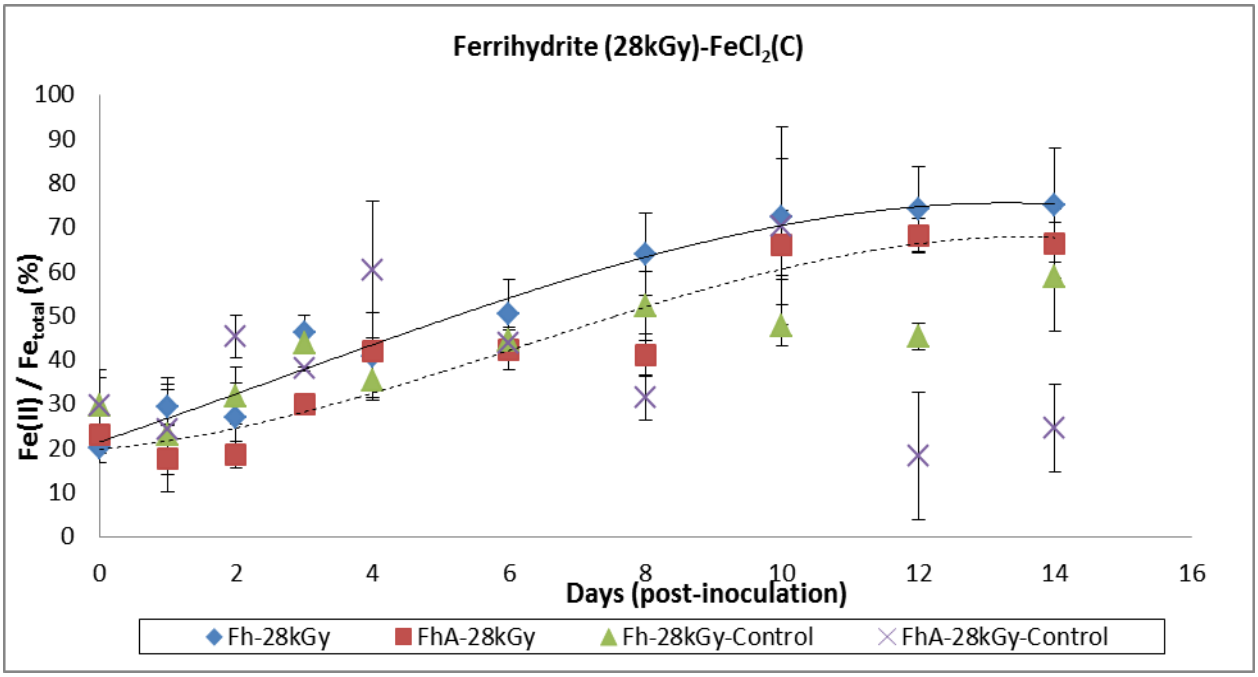

Figure C-1: Quality control experiments comparing the use of a ferric nitrate salt solution versus a ferric nitrate salt during the synthesis. Changes to total Fe (II)/total Fe during the reduction of (A) Ferrihydrite (Fh) and Ferrihydrite + Alginate (FhA) and Fh and FhA subjected to sterilization using gamma irradiation at (B) 5kGy and (C) 28 kGy by *S. putrefaciens* CN32. Data markers represent means and standard deviations of 3 replicate experiments. Solid lines represent 3-parameter sigmoid lines of best fit to the data for Fh data and the dashed lines represent 3-parameter sigmoid lines of best fit to the data for FhA. Correlation coefficient (R^2) of the fitted lines are (A) Fh=0.986, FhA=0.943, (B) Fh=0.965, FhA=0.962, and (C) Fh=0.916, FhA=0.911.

Appendix D: Kostka and Luther (1994) Chemical extraction protocol for Iron Oxides

0.5 M HCl Extraction

Under anaerobic conditions, 10 mL 0.5 M HCl was added to ≈0.02g of wet iron oxide samples (in triplicates) using clean 20 mL, scintillation vials and the addition of a magnetic stir bar. Samples were stored in an anaerobic chamber to stir for 1 hour. To determine the Fe (II) concentration of a sample, 100 µL of the chemical extract was added to 5 mL of "diluted" ferrozine (12 g of 4-(2-hydroxyethyl)-1-piperazineethanesulfonic acid) (HEPES) and 1 g of ferrozine added to 900 mL of ultrapure water) in 15 mL falcon tube and vortexed (10 seconds). After, 20-30 minutes samples, add 100 µL of "concentrated" ferrozine (0.5 g of ferrozine in 100mL of ultrapure water) to the previous 15 mL falcon tube and let stand for another 20-30 minutes (total volume in falcon tube is 5200 µL). To determine the amorphous iron oxide within the sample, add 100 µL of HCl extract to 5 mL hydroxylamine/HEPES solution (add 0.2 g of hydroxylamine and 1.2 g of HEPES to 100 mL of ultrapure water). After 30 minutes, add 100 µL of the concentrated ferrozine to the extract and hydroxylamine/HEPES solution and vortex. All samples (Fe (II) and amorphous iron) were then filtered using 0.2 µm Puradisc disposable syringe filters and then 900 µL of solution was transferred to a 1.5 mL cuvette and the absorbance was determined using the Ultraspec 1100 spectrophotometer (set wavelength at 562 nm). The absorbance values were then applied to Beers Law equation. *All absorbance values obtained from each chemical extraction were applied to the Beers law.

Oxalate Extraction

Prior to the chemical extraction, all 20 mL scintillation sample vials, 100 mL solution bottles and 15 mL falcon tubes were wrapped in foil because as mentioned by Kostka and Luther III (1994), oxalate is light sensitive and if exposed, it will transform to a reducing agent. Solution preparation (Solution C) for this extraction involves a mixture of two solutions. Solution A contains 2.842 g of ammonium oxalate monohydrate and 100 mL of ultrapure water. Solution B contains 2.522 g of oxalic acid dehydrate and

100 mL ultrapure water. Both solutions A and B are made in 100 mL clean Pyrex bottle with clean magnetic stir bar and stirred for 30 minutes. In a third bottle, Solution C consists of 56.82 mL of solution A and 43.2 mL of solution B. Approximately, 0.01 g of iron oxide sample was weighed out in the prepped scintillation vials and a clean stir bar was added along with 10 mL of solution C, capped and placed in the anaerobic chamber for 24 hours. After 24 hours, using prepped 15 mL falcon tubes follow the same procedures as the 0.5 M HCl extraction (using the oxalate extract) to determine the amount of Fe(II) and amorphous within the iron oxide samples.

Ascorbate Extraction

100 mL of extraction solution was prepared by adding 5.698 g of sodium citrate dihydrate and 5.000 g if sodium bicarbonate to 100 mL of ultrapure water and solution was mixed until full dissolution. The mixture was then bubbled with N_2 gas. The bottle was wrapped in aluminum foil to prevent the direct contact with sunlight followed by the addition of two grams ascorbic acid within the anaerobic chamber and ensure the pH is 8.0. Ten millilitres of solution was added to iron oxide samples (same sample mass used in HCl extractions) and the extraction is stirred for 48 hours before the solution is subjected to ferrozine to determine the amorphous iron (follow the same procedures as the 0.5 M HCl extraction).

Dithionate Extraction

To dissolve the more crystalline structures such as goethite and lepidocrocite , within a fume hood, 2 mL of 18 M (Glacial) acetic acid was added to 98 mL of ultrapure water followed by the addition of 5.882 g of sodium citrate dihydrate to the acetic acid solution (pH should be 4.8). In a 20 mL scintillation vial a stir bar, ≈0.0200g of iron oxide sample, and 10 mL of acetic acid solution were added and the mixture was vortexed. Vials were then placed in the oven at 70^{o}C for 1 hour. After the 1 hour mark, 0.5 g of sodium dithionite was rapidly added directly to hot solution and mixed. It is important to not let the solution cool prior to adding the sodium dithionite. Vials were then placed into the oven for

another hour (occasionally swirl solution to ensure proper dissolution). Samples were cooled and 100 µL of chemical extract was added to 5 mL of diluted ferrozine for 20-30 minutes and then the final solutions were filtered and absences were determined.

Strong HCl Total Fe Extraction

To determined total iron, 20 mL of 12 M HCl was added to a known mass of iron oxide (≈0.1 g) in a clean 20 mL scintillation vial with a stir bar and stirred for 1 hour. During this time, within 20 mL scintillation vials, 4.5 mL of a hydroxylamine solution (0.2 g of hydroxylamine and 1.2 g of HEPES were added to 100 mL 0.5 M HCl) was added. A serial dilution was carried out (10x, 100x, and 1000x) from the concentrated HCl samples. Once the serial dilution was completed, vials were capped tightly and vortexed. Vials were then transferred to a 1 L beaker (excluding the vials with 12 M HCl) with water and brought to boil for 3 hours. Post extraction, 100 µL of sample was added to 4.9 mL of diluted ferrozine and the absorbance was calculated.

Appendix E: Sample protocol for Microcosm Experiments created by Dr. Sean Langley-Characterization and Microbial Reduction of Bacteriogenic Iron Oxides (2009).

Preparation of Anoxic Water

1. Fill a 1.5 or 2 L acid-washed beaker with 1 L of ultrapure water and cover it with aluminum foil.

2. While bubbling the water with 100% nitrogen, bring the water to a rolling boil for 5 minutes.

3. Remove the water from the hotplate, but maintain the nitrogen flow.

4. While still bubbling with N_2, allow the water to cool until it can just be held against your bare skin. It should still feel hot, without burning.

5. Remove the nitrogen tube and immediately transfer the water to an acid-washed 1 L serum bottle.

6. Cap the bottle loosely and immediately transfer it into the anaerobic chamber.

Notes: adequate cooling in step 4 is essential. If the water is too hot, it can boil over (violently) inside the chamber airlock when the vacuum is applied. When you start the airlock cycle, keep a close eye on the water for any sign of boiling as the vacuum builds. If boiling starts, immediately turn off the vacuum and equalize the airlock pressure with nitrogen. Then wait for the water to cool some more and try again.

However, oxygen solubility in water decreases with increasing temperature, so don't let the water cool all the way back down to room temperature in air, or it will re-absorb a significant amount of oxygen.

Tips: it's a very good idea to maintain a backup supply of anoxic water within the chamber at all times, especially for rinsing the redox electrode after taking measurements. If you don't use anoxic rinse water between measurements, the electrode will take much longer to equilibrate when placed in your reduced samples.

It's always best to leave the bottle open in the chamber overnight before using the water, to insure that all trace oxygen has diffused out.

Despite the point above, always be sure to keep water (or any aqueous solution) in a sealed bottle inside the chamber, otherwise excessive humidity can develop. This will decrease the effectiveness of the dessicant and oxygen-scrubbing catalysts within the chamber.

Preparation of BIOS Microcosm Bottles

This procedure is carried out on the bench, not inside the anaerobic chamber.

1. Prepare a 10x concentration of phosphate solution, based on the recipe of the growth medium to be used.

2. Prepare the growth medium, but *do not* include the necessary phosphate. Phosphate will be added from the 10x stock solution, after autoclaving. So, if preparing 1 L of medium, dissolve all of the powders or solutions into 900 mL of water. The final 100 mL will come from addition of the phosphate solution.

3. For every 1 L serum bottle to be used, you will need 700 mL of complete medium.

4. Dispense 630 mL of medium into each 1 L serum bottle and cap the bottle loosely. Also, dispense 70 mL of phosphate stock solution into each 125 mL beaker. Cover the top of the beaker with aluminum foil. Send all of the bottles and beakers to be autoclaved (wet cycle).

5. When cool, using aseptic technique, add the phosphate solution to the serum bottle, keeping the beaker and foil sterile for later use.

Note: if the phosphate is added prior to autoclaving (or if it is added before the solutions have cooled sufficiently) the phosphate will precipitate with the Ca and Mg in the medium and you will have to start over.

6. Using a sterile spatula and aseptic technique, homogenize a tube of BIOS as thoroughly as possible. Then, weigh out a sufficient mass of wet BIOS to give 4 mM total iron in 700 mL of medium. Weigh this quantity directly into the sterile beaker that was used to autoclave the phosphate solution.

7. Using aseptic technique, pour some of the medium from a serum bottle into the beaker and swirl it gently to resuspend the BIOS. While the BIOS is still suspended, carefully pour the suspension back into the serum bottle. Repeat this process as necessary, until all of the BIOS has been added into the serum bottle. When done, cap the bottle loosely, swirl it gently to mix all of the BIOS and phosphate completely into the medium, and transfer the bottle into the anaerobic chamber.

8. Take your “Time zero” measurements and samples immediately after getting the bottles into the chamber.

Procedure for Sampling Inside the Anaerobic Chamber

For each serum bottle to be sampled, you will need the following items inside the chamber:

Notes: all screw caps must be loosened before placing inside the chamber airlock, to allow for adequate gas exchange. Sterile microfuge tubes should go through the chamber airlock with their caps fully inserted, to prevent contamination of the tubes.

Full squeeze bottles must be fully uncapped before placing inside the chamber airlock, otherwise all of the water will be expelled during the vacuum stage of airlock operation.

One sterile 20 mL scintillation vial

One 5 mL pipette, calibrated to deliver 3 mL

One 5 mL pipette, calibrated to deliver 4 mL

Two non-sterile, 20 mL scintillation vials (*must be new and, preferably, also acid-washed*)

One 1 mL pipette, calibrated to deliver 0.5 mL

One 1 mL pipette, set to deliver 1 mL

Sterile 1 mL pipet tips

Sterile 5 mL pipet tips

Two 15 mL plastic centrifuge tubes, each filled with 4.5 mL of 0.5 N HCl

One sterile 1.5 mL microfuge tube

Two 15 mL plastic centrifuge tubes

One 10 mL syringe

One syringe filter

One 3 mL syringe, with fine gauge needle (black or green box)

One 2 mL amber vial, containing 0.12 mL of complete Cline's sulfide reagent

One portable pH meter and probe, *calibrated before placing into the chamber*

One portable redox meter and probe, *calibrated before placing into the chamber*

Squeeze bottle filled with ultrapure water (preferably anoxic)

Beaker (400 or 600 mL) for collecting waste water

Larger beaker (1 L) for collecting garbage and spent supplies (used syringes, paper towels, etc)

Sharpie, or other permanent, fine-tipped marker

Paper and pen/pencil

1. Swirl the serum bottle to completely re-suspend the BIOS.

2. While the BIOS is still in suspension, and being as aseptic as possible, pour some of the suspension into the sterile 20 mL scintillation vial, filling it just up to the neck of the vial, then immediately re-cap the serum bottle. From this point on, you will be working only from the scintillation vial. Whenever necessary, swirl the vial gently to keep the BIOS in suspension.

3. With the BIOS in suspension, using a sterile pipet tip, transfer 1 mL of the suspension into the sterile 1.5 mL microfuge tube, and cap the tube. This tube can be used for enumeration of Fe-reducing organisms, if desired.

4. With the BIOS in suspension, transfer 0.5 mL of suspension into one of the 0.5 N HCl tubes. Cap the tube tightly and shake to mix well. Label this tube "total". Leave this tube inside the chamber for at least 24 hours before measuring Fe(II) according to the ferrozine procedure.

5. With the BIOS in suspension, transfer 6 mL of suspension into one of the non-sterile 20 mL scintillation vials. Cap the vial and label it as "total".

6. With the BIOS in suspension, pour all of the remaining suspension from the sterile scintillation vial into one of the empty 15 mL centrifuge tubes, and cap the tube *as tightly as possible*.

7. Remove the centrifuge tube from the chamber and *immediately* centrifuge it at maximum rpm for 5 minutes. When the centrifuge cycle is complete, *immediately* transfer the tube back into the chamber, being careful not to disturb the pellet during the process.

8. Back in the chamber, remove the plunger from the 10 mL syringe, and attach the syringe filter to the tip of the syringe.

9. Carefully pour about 6 mL of the supernatant fluid from the centrifuged sample into the open end of the syringe.

10. While holding the tip of the syringe filter into an empty 20 mL scintillation vial, insert the plunger back into the syringe and completely filter all of the solution into the vial.

11. Remove the syringe filter and leave it on top of the vial, then remove the plunger from the syringe again.

12. Pour all of the remaining supernatant fluid into the syringe (being careful not to disturb the pellet too much) and filter it into the vial as before.

13. Transfer 0.5 mL of filtered sample into one of the 0.5 N HCl tubes. Cap the tube tightly and shake to mix well. Label this tube "soluble". Leave this tube inside the chamber for at least 24 hours before measuring Fe(II) according to the ferrozine procedure.

14. Transfer 4 mL of filtered sample into an empty 15 mL centrifuge tube. This sample can be used for the determination of soluble phosphate, if desired.

15. Using a 3 mL syringe and needle, transfer 1.5 mL of filtered sample into a capped 2 mL amber vial containing Cline's sulfide reagent. Shake the amber vial thoroughly to mix the reagent and sample completely. The vial can then be removed from the chamber to read the absorbance of the mixture.

16. The remaining 6 mL of filtered sample can now be capped. Label this vial as "soluble".

Measure pH and redox potential (Eh)

17. Swirl the serum bottle to completely re-suspend the BIOS.

18. Being as aseptic as possible, pipet 4 mL of the BIOS suspension from the serum bottle into the 15 mL centrifuge tube that you used in steps 6 and 7 above, then immediately re-cap the serum bottle. Shake the tube to re-suspend the pellet.

19. Remove the pH probe from the storage solution and rinse it thoroughly with anoxic ultrapure water from the squeeze bottle.

20. Insert the probe into the centrifuge tube, ensuring that the bulb is completely immersed in the BIOS suspension. Swirl the tube gently until a stable pH reading is obtained. Note the reading.

21. Rinse the pH probe thoroughly and return it to the storage solution.

22. Repeat this procedure using the redox meter and probe. Be aware that the redox measurements can take a *very long* time to stabilize, so swirl the tube gently only for the first few seconds, then let the probe sit in the solution for as long as it takes to stabilize. Note the reading.

Appendix F: Mossbauer analyzed by Dr. Yoichi Sakai Daido and Dr. Yoshio Takahashi at the University of Tokyo, Japan.

Massbauer for F+A,G sample at 78K by Dr. Sakai
The spectraum shows only the presence of Fe^{3+}.

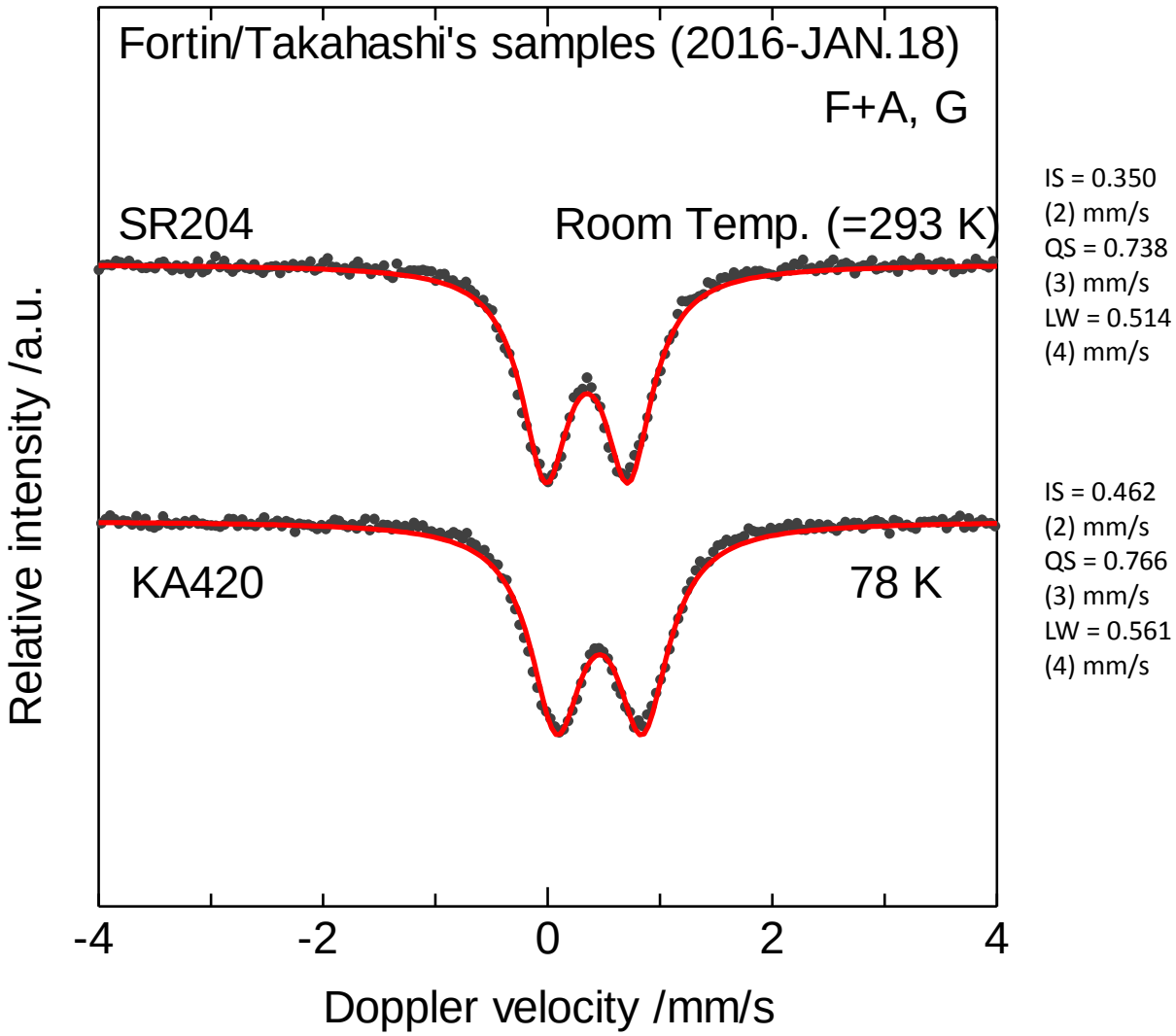

Room Temperature (293 K)

F = ferrihydrite
A = alginate
G = gamma-ray (28 kGy)

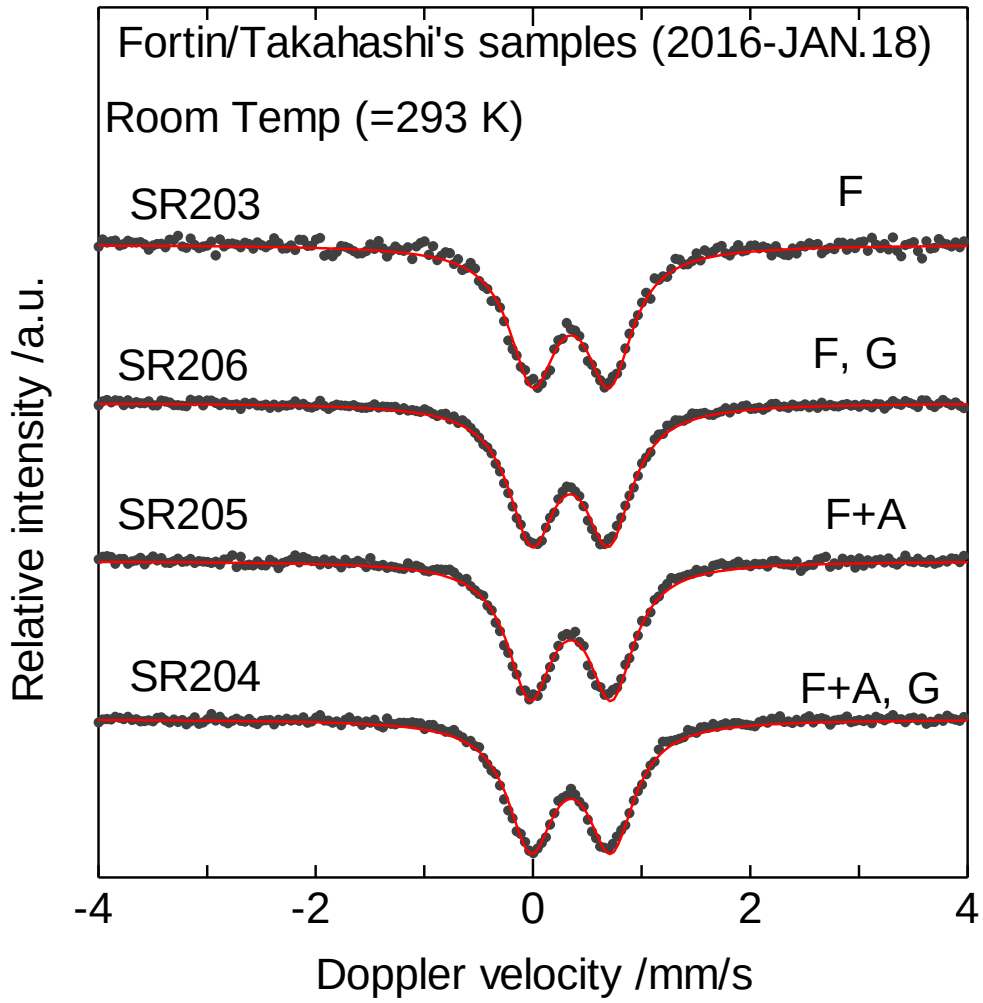

IS = 0.351 (3) mm/s
QS = 0.703 (5) mm/s
LW = 0.519 (7) mm/s

IS = 0.344 (1) mm/s
QS = 0.704 (2) mm/s
LW = 0.522 (3) mm/s

IS = 0.347 (2) mm/s
QS = 0.748 (3) mm/s
LW = 0.502 (4) mm/s

IS = 0.350 (2) mm/s
QS = 0.738 (3) mm/s
LW = 0.514 (4) mm/s

Appendix G: Colour Characterization of Ferrihydrite, Lepidocrocite, and Goethite indicated from Cornell and Schwertmann (2000) followed for samples used for this study.

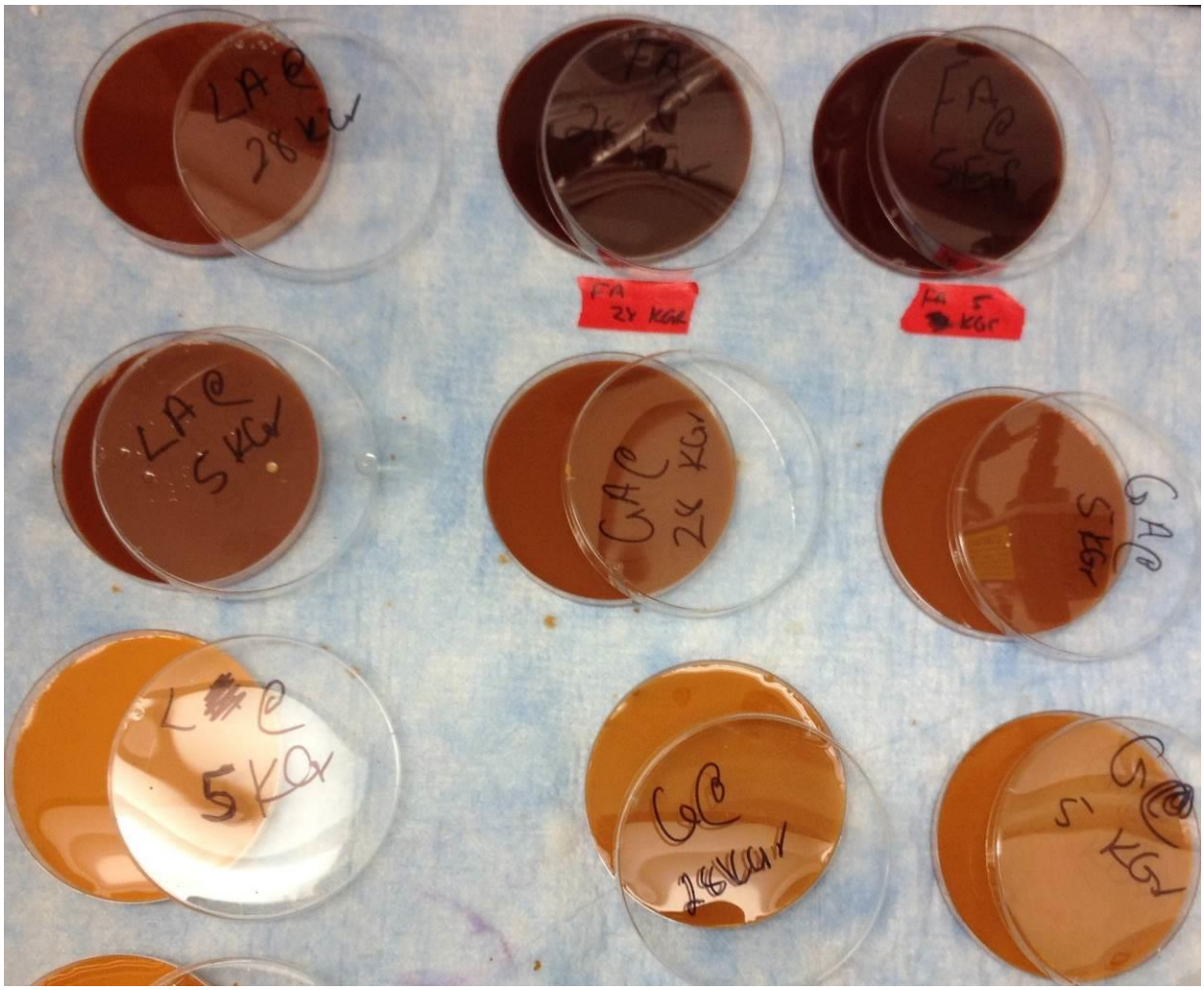
LAC
28 KGy
FA
2y KGy
FA
5 KGy
LAC
5KGy
CAC
2y KGy
CAC
5KGy
LAC
5KGy
CAC
28KGy
CAC
5 KGy

Appendix H: Ferrihydrite and Ferrihydrite +Alginate analysis for Nitrate (NO_3^-) using Ion Chromatography carried out at the University of Ottawa by Dr. Nimal De Silva and Ping Zhang.

November 3rd, 2015

Inj. NO3	Injection Name NO3	Type NO3	Amount NO3 ppm		
1	blank	Blank	n.a.		
2	blank	Blank	n.a.		
3	0.62	Calibration Standard	0.5179		
4	1.25	Calibration Standard	1.1059		
5	2.5	Calibration Standard	2.3727		
6	5	Calibration Standard	5.1131		
7	blank	Unknown	0.0016		
8	blank	Unknown	0.0027		
	average		0.00215		
	STDEV		0.00078		
	LOD		0.00233		
				Dilution factor	corrected
9	check 0.1ppm	Unknown	0.102	Ping diluted	
10	k1	Unknown	0.0041		0.0020
11	k2	Unknown	n.a.		
12	k3	Unknown	n.a.		
13	k4	Unknown	n.a.		
14	k5	Unknown	n.a.		
15	k6	Unknown	n.a.		
16	k7	Unknown	n.a.		
17	k8	Unknown	n.a.		
18	k9	Unknown	n.a.		
19	k10	Unknown	n.a.		
20	k11	Unknown	n.a.		
21	k12	Unknown	n.a.		
22	k13x5	Unknown	n.a.	5	
23	k14	Unknown	n.a.		
24	k15	Unknown	n.a.		
25	k16x2	Unknown	0.9878	2	1.9756
26	k17	Unknown	n.a.		
27	k18	Unknown	n.a.		
28	k19	Unknown	n.a.		
29	k20	Unknown	n.a.		
30	K2 x100	Unknown	0.0392	100	3.92
31	k2 x50	Unknown	0.0859	50	4.295
32	k2 x10	Unknown	0.4449	10	4.449
33	k21	Unknown	n.a.		
34	k22	Unknown	n.a.		
35	k23	Unknown	n.a.		
36	k24	Unknown	n.a.		
37	k25	Unknown	n.a.		
38	k26	Unknown	n.a.		
39	k27	Unknown	n.a.		
40	k28	Unknown	n.a.		

41	k29	Unknown	n.a.		
42	k30	Unknown	n.a.		
43	k31	Unknown	n.a.		
44	k32	Unknown	n.a.		
45	k33	Unknown	n.a.		
46	k34	Unknown	n.a.		
47	k35	Unknown	n.a.		
48	k36	Unknown	n.a.		
49	k37	Unknown	n.a.		
50	k38	Unknown	n.a.		
51	k39	Unknown	n.a.		
52	blank	Unknown	n.a.		
53	blank	Unknown	n.a.		

November 10th, 2015

Inj. NO3	Injection Name NO3	Type NO3	Amount NO3 ppm		
1	blank	Blank	n.a.		
2	0.62	Calibration Standard	0.5218		
3	1.25	Calibration Standard	1.0987		
4	2.5	Calibration Standard	2.3592		
5	5	Calibration Standard	5.1211		
6	blank	Unknown	n.a.		
7	blank	Unknown	n.a.		
				Dilution factor	corrected
8	check 0.12ppm	Unknown	0.102	Brandon diluted	
9	k1X20	Unknown	0.5922	20	11.844
10	k2X20	Unknown	n.a.	20	
11	k3x20	Unknown	0.2849	20	5.698
12	check 6 anions (0.1ppm)	Unknown	0.1026	20	
13	k4x20	Unknown	0.3094	20	6.188
14	k5x20	Unknown	n.a.	20	
15	k6x20	Unknown	n.a.	20	
16	k7x20	Unknown	n.a.	20	
17	k8x20	Unknown	n.a.	20	
18	k9x20	Unknown	n.a.	20	
19	k10x20	Unknown	n.a.	20	
20	k11x20	Unknown	n.a.	20	
21	k12x20	Unknown	n.a.	20	
22	k13x20	Unknown	n.a.	20	
23	k14x20	Unknown	n.a.	20	
24	k15x20	Unknown	n.a.	20	
25	k16x20	Unknown	n.a.	20	
26	k17x20	Unknown	n.a.	20	
27	k18x20	Unknown	n.a.	20	
28	k19x20	Unknown	n.a.	20	
29	k20x20	Unknown	n.a.	20	
30	blank	Unknown	n.a.		

31	blank	Unknown	n.a.		
32	k21x20	Unknown	n.a.	20	
33	k22x20	Unknown	n.a.	20	
34	k23x20	Unknown	n.a.	20	
35	k24x20	Unknown	n.a.	20	
36	k25x20	Unknown	n.a.	20	
37	k26x20	Unknown	n.a.	20	
38	k27x20	Unknown	n.a.	20	
39	k28x20	Unknown	n.a.	20	
40	k29x20	Unknown	n.a.	20	
41	k30x20	Unknown	n.a.	20	
42	k31x20	Unknown	n.a.	20	
43	k32x20	Unknown	n.a.	20	
44	k33x20	Unknown	n.a.	20	
45	k34x20	Unknown	n.a.	20	
46	k35x20	Unknown	n.a.	20	
47	k36x20	Unknown	n.a.	20	
48	k37x20	Unknown	n.a.	20	
49	k38x20	Unknown	n.a.	20	
50	k39x20	Unknown	n.a.	20	
51	k40x20	Unknown	n.a.	20	
52	blank	Unknown	n.a.		
53	blank	Unknown	n.a.		